HHS Public Access

Author manuscript

Cell Rep. Author manuscript; available in PMC 2023 May 07.

Published in final edited form as:

Cell Rep. 2023 March 28; 42(3): 112230. doi:10.1016/j.celrep.2023.112230.

FAM193A is a positive regulator of p53 activity

Maria M. Szwarc[1,6], **Anna L. Guarnieri**[1,6], **Molishree Joshi**[1,2], **Huy N. Duc**[2], **Madison C. Laird**[2], **Ahwan Pandey**[1,3], **Santosh Khanal**[1], **Emily Dohm**[1], **Aimee K. Bui**[1], **Kelly D. Sullivan**[1,4,5], **Matthew D. Galbraith**[1,4], **Zdenek Andrysik**[1,4,*], **Joaquin M. Espinosa**[1,2,4,7,*]

[1]Department of Pharmacology, University of Colorado Anschutz Medical Campus, Aurora, CO 80045, USA

[2]Functional Genomics Facility, University of Colorado Anschutz Medical Campus, Aurora, CO 80045, USA

[3]Peter MacCallum Cancer Centre, Melbourne, VIC 3000, Australia

[4]Linda Crnic Institute for Down Syndrome, University of Colorado Anschutz Medical Campus, Aurora, CO 80045, USA

[5]Department of Pediatrics, Section of Developmental Biology, University of Colorado Anschutz Medical Campus, Aurora, CO 80045, USA

[6]These authors contributed equally

[7]Lead contact

SUMMARY

Inactivation of the p53 tumor suppressor, either by mutations or through hyperactivation of repressors such as MDM2 and MDM4, is a hallmark of cancer. Although many inhibitors of the p53-MDM2/4 interaction have been developed, such as Nutlin, their therapeutic value is limited by highly heterogeneous cellular responses. We report here a multi-omics investigation of the cellular response to MDM2/4 inhibitors, leading to identification of FAM193A as a widespread regulator of p53 function. CRISPR screening identified FAM193A as necessary for the response to Nutlin. FAM193A expression correlates with Nutlin sensitivity across hundreds of cell lines. Furthermore, genetic codependency data highlight FAM193A as a component of the p53 pathway across diverse tumor types. Mechanistically, FAM193A interacts with MDM4, and FAM193A depletion stabilizes MDM4 and inhibits the p53 transcriptional program. Last,

*Correspondence: zdenek.andrysik@cuanschutz.edu (Z.A.), joaquin.espinosa@cuanschutz.edu (J.M.E.).

AUTHOR CONTRIBUTIONS

M.M.S., A.L.G., Z.A., M.J., K.D.S., M.D.G., and J.M.E. designed experiments. M.M.S., A.L.G., Z.A., M.J., H.N.D., M.C.L., E.D., and A.K.B. prepared reagents and performed experiments. M.M.S., A.L.G., Z.A., A.P., S.K., and M.D.G. analyzed data. M.M.S., A.L.G., Z.A., K.D.S., M.D.G., and J.M.E. interpreted data. M.M.S., A.L.G., Z.A., M.D.G., and J.M.E. wrote the manuscript. All authors reviewed and edited the manuscript. J.M.E. provided oversight and intellectual leadership to the project.

DECLARATION OF INTERESTS

J.M.E. has provided consulting services for Elli Lily and Co. and Gilead Sciences Inc. and serves on the advisory board of Perha Pharmaceuticals and on the editorial board of *Cell Reports.*

SUPPLEMENTAL INFORMATION

Supplemental Information can be found online at https://doi.org/10.1016/j.celrep.2023.112230.

FAM193A expression is associated with better prognosis in multiple malignancies. Altogether, these results identify FAM193A as a positive regulator of p53.

In brief

Szwarc et al. identify FAM193A as a positive regulator of the tumor suppressor p53. Using genetic screening, FAM193A is found to be required for the cellular response to targeted p53 activation. FAM193A interacts with the p53 repressors MDM2 and MDM4, destabilizes MDM4, and enhances p53 activity as a transcription factor.

Graphical abstract

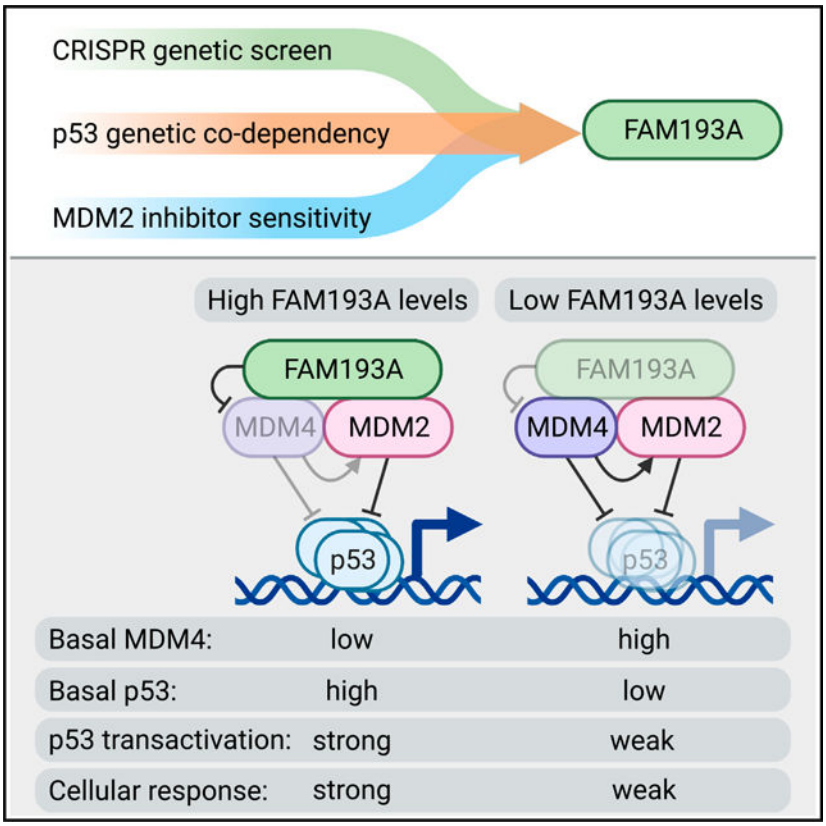

INTRODUCTION

The critical role of the *TP53* tumor suppressor gene in cancer biology is undisputed, as underscored by the fact that nearly a third of all human cancers carry mutations in the *TP53* locus.[1–3] *TP53* encodes a transcription factor that exerts tumor suppression via downstream transcriptional programs driving diverse cellular processes with anti-tumoral potential, including but not restricted to cell-cycle arrest, senescence, apoptosis, autophagy, and metabolic control.[4–6] Activation of p53 is triggered by various cellular stress stimuli, such as DNA damage, oncogene activation, and nutrient deprivation, which alleviate the effects of endogenous p53 repressors, including the homologous proteins Mouse Double Minute 2 (MDM2) and MDM4.[4] While MDM2 inhibits p53 function by masking its transactivation

domain and by targeting p53 for ubiquitin-dependent proteasomal degradation through its E3 ubiquitin ligase activity,[7,8] MDM4 also directly impedes p53-dependent transactivation, but it does not directly ubiquitinate p53.[9,10] Noteworthy, the *MDM2* gene, but not *MDM4,* is a direct transcriptional target of p53, thus creating a negative feedback loop that tightly regulates p53 activity.[11] In mice, germline knockout of either *Mdm2* or *Mmd4* is embryonic lethal, and the phenotype is rescued by loss of p53, thus confirming the critical role of both repressors in controlling p53 function.[12–16] However, there is evidence supporting the notion that MDM2 and MDM4 play context-specific roles in repressing p53 in different adult tissues.[17–20]

Given that over half of tumors retain wild-type p53, significant effort has been devoted to the design and testing of pharmacological approaches to reactivate dormant p53 for cancer therapy, most prominent among them are small-molecule inhibitors of the interaction between the p53 transactivation domain and the p53-binding surfaces of MDM2 and/or MDM4. Since the initial discovery of the first-in-class molecule Nutlin-3,[21] many other small molecules and stapled peptides have been developed (reviewed in Sanz et al.[22]). Although these agents effectively activate p53 and downstream transcriptional responses, their therapeutic value as monotherapies has been very limited so far. In most cancer cell types tested, p53 reactivation with these molecules leads to cell-cycle arrest, a reversible response of little therapeutic benefit.[23] Accordingly, in cell culture and in clinical trials, drug resistance appears rapidly via selection of p53 mutant cell clones.[6,24–27] Regardless of cellular outcome upon MDM2 inhibition, p53 consistently activates a multi-functional transcriptional program with dozens of target genes involved in diverse, often counteracting, signaling pathways.[6,28] Whether cells undergo rapid cell death upon p53 activation seems to be defined by a large number of variables, including configuration and activity of the cell cycle machinery,[29,30] expression and activity of components of the BCL2-BH3) apoptosis control network,[31,32] activity of other transcription factors co-regulating p53 target genes,[33] and redox metabolic state,[34] to name a few. This complexity of the control of the cellular response to p53 activation has prevented the identification of clinically useful biomarkers of sensitivity and combinatorial therapies.

To gain further insight into mechanisms defining cell fate choice upon p53 activation and response to MDM2/4 inhibitors, we first completed a comprehensive analysis of Nutlin sensitivity across hundreds of cancer cell lines, which revealed that sensitivity is associated with high basal activity in the p53 transcriptional network before drug treatment. This analysis led us to identify and characterize one of the most Nutlin-sensitive cell lines, the neuroblastoma cell line CHP212, which we then used in a CRISPR genetic screen to identify factors required for the Nutlin-induced cellular response. This screen identified 54 high-confidence hits, including *TP53* itself and its target gene *BBC3* (PUMA), a known mediator of p53-dependent apoptosis.[35,36] Through various complementary analyses, we identified the screen hit FAM193A as a key positive regulator of p53 function. FAM193A expression is correlated with Nutlin sensitivity across hundreds of cell lines, and genetic codependency analysis revealed a strong positive genetic interaction between p53 and FAM193A across vastly diverse tumor cell types. Loss of FAM193A leads to MDM4 stabilization, lower p53 protein expression, attenuation of the p53 transcriptional program, and survival upon Nutlin treatment. Importantly, FAM193A interacts with the RING domain of MDM4 and forms a

ternary complex with MDM2 and MDM4. Last, FAM193A expression is associated with good prognosis in diverse cancer types. Altogether, these results identify FAM193A as a widespread positive regulator of p53 function.

RESULTS

Sensitivity to MDM2 inhibitors is associated with strong basal activity in the p53 network

To investigate mechanisms defining the cellular response to non-genotoxic p53 reactivation with MDM2 inhibitors, we analyzed a dataset available at the Genomics of Drug Sensitivity in Cancer (GDSC) database.[37] As part of the GDSC efforts, Nutlin-3 was tested on 492 cell lines representing all major tumor types for which *TP53* status was defined (i.e., 179 wild-type *TP53* versus 313 *TP53* mutant) (Table S1). Expectedly, when we partitioned cell lines by *TP53* mutational status, *TP53* mutant cell lines show significantly higher IC_{50} values (Figure 1A). However, wild-type *TP53* cell lines display a wide range of sensitivity, often within the range of *TP53* mutant cell lines, indicating the existence of mechanisms strongly affecting the cellular response to p53 activation with Nutlin. In early clinical trials, *MDM2* amplification, which is present in more than 90% of liposarcomas, was assumed to be a biomarker of sensitivity.[38] However, on average, cell lines with wild-type *TP53* and *MDM2* amplification present in the GDSC dataset do not display significantly lower IC_{50} values (Figures 1B and S1). Among cell lines with *MDM2* amplification, the well-characterized SJSA1 cell line displays a low IC_{50} value, but many cell lines without *MDM2* amplification (e.g., CHP212), are even more sensitive (Figure 1B), supporting the notion that *MDM2* amplification is not a clinically actionable biomarker of sensitivity.[39]

Next, to investigate the potential mechanisms driving this large phenotypic diversity among wild-type *TP53* cell lines, we employed the transcriptome data available in the GDSC dataset to rank genes by correlation between their basal expression (i.e., in the absence of any drug treatment) and Nutlin IC_{50} values (Figure 1C; Table S2). Interestingly, top-ranking genes associated with Nutlin sensitivity are well-known direct p53 target genes, including *MDM2* itself (e.g., *AEN, CYFIP2, DDB2, BAX, EDA2R, XPC, RPS27L,* and *ZMAT3)* (Figures 1C and 1D). This observation may seem paradoxical because *MDM2* amplification status did not predict sensitivity. However, in this context, *MDM2* is part of a larger signature of p53 target genes whose expression correlates with Nutlin sensitivity. To probe this further, we analyzed the top genes associated with Nutlin sensitivity with Ingenuity Pathway Analysis (IPA) (i.e., top 100, top 250, top 500, and top 1,000). The IPA Upstream Regulator tool identified p53 and its related factor p73 as the most likely drivers of the top 100 gene signature (Figure 1E). Thus, high basal expression of p53 target genes is clearly associated with Nutlin sensitivity. Furthermore, when we position in this ranking a curated list of 103 high-confidence direct p53 target genes identified by GRO-seq measurements at short time points of Nutlin treatment in diverse cancer cell types,[6] it is clear that basal expression of this core p53 transcriptional program is significantly associated with Nutlin sensitivity (Figure 1F). This result reinforces a previous report identifying a 13-gene signature composed of direct p53 target genes as predictive of sensitivity to a structurally different MDM2 inhibitor, the Novartis compound NVP-CFC218.[41] In fact, this 13-gene signature is clearly enriched among genes positively correlated with sensitivity to Nutlin in

our analysis of the GDSC dataset (Figure 1F). During studies of a third MDM2 inhibitor, the Daichi compound DS3032b, a 175-gene signature was identified to predict sensitivity to this drug.[40] Of note, this 175 gene-signature is also highly enriched for direct p53 target genes, including all 13 genes in the biomarker predictive of sensitivity to NVP-CFC218, and is also significantly enriched among genes whose expression is associated with Nutlin sensitivity in the GDSC dataset (Figure 1F).

Altogether, these results indicate that sensitivity to three structurally different MDM2 inhibitors is associated with strong basal activity in the p53 network, suggesting that the response to Nutlin could be determined by cellular factors that modulate the overall strength of the p53 transcriptional program in cells harboring wild-type *TP53*.

A CRIPSR screen identifies regulators of the cellular response to p53 activation

Next, we decided to characterize the cellular response to Nutlin for a select set of wild-type *TP53* cell lines with a wide range of predicted Nutlin sensitivities according to the GDSC dataset, including A549 (lung carcinoma), MCF7 (breast adenocarcinoma), HCT116 (colorectal carcinoma), SJSA1 (osteosarcoma), and CHP212 (neuroblastoma) cell lines (highlighted in Figure 1B). Nutlin treatment caused strong stabilization of p53 and induction of its target genes CDKN1A/p21 and BBC3/PUMA in all five cell lines (Figures 2A and S2A). However, the apoptotic response was highly variable, with CHP212 cells showing the strongest apoptotic phenotype, even above that observed for SJSA1 cells, a well-characterized osteosarcoma cell line with *MDM2* amplification (Figures 2A and 2B). Expectedly, SJSA1 cells, but not the other cell lines, show greatly increased levels of MDM2 (Figure 2A). A comparative time-course analysis of SJSA1 versus CHP212 cells showed that CHP212 cells launch an earlier apoptotic response (Figure S2A). Thus, the CHP212 cell line provides a suitable model to identify factors driving Nutlin sensitivity in the absence of *MDM2* amplification.

To elucidate mechanisms driving Nutlin sensitivity, we performed a loss-of-function CRISPR-based genetic screen in the CHP212 cell line (Figure S2B). CHP212 cells were transduced with the GeCKO v.2 library[43] carrying 121,411 gRNAs targeting 20,915 human genes plus 1,000 non-targeting control sgRNAs. After library transduction and selection, cells were cultured for 10 days to clear from the population any cells carrying sgRNAs targeting essential genes. After this clearance step, cell cultures were treated with either 10 μM Nutlin-3a or vehicle (DMSO) for 48 h, allowed to recover for 10 days, treated with a second round of Nutlin or DMSO, and allowed to recoveragain. After the second recovery step, genomic DNA was purified and used for PCR-based amplification of sgRNA cassettes for next-generation sequencing analysis (Figure S2C; see STAR Methods for details). Analysis of sgRNA abundance revealed a massive overall loss of sgRNAs as expected by the apoptotic response elicited by Nutlin inCHP212, including the bulkof non-targeting sgRNAs (Figure 2C, Table S3). However, a minor fraction of sgRNAs was enriched in Nutlin-treated cells, which would likely target genes mediating sensitivity to Nutlin (Figure 2C). To identify high-confidence screen hits, we required 2-fold enrichment in sgRNA counts and a minimum of 2 enriched sgRNAs per gene, which produced a list of 54 candidate genes (Figure S2C; Table S3). Unsurprisingly, *TP53* itself ranked at the top of this list, with all

6 sgRNAs in the library targeting *TP53* being significantly enriched (Figures 2C and S2D). Reassuringly, *BBC3* (PUMA), a known modulator of p53-dependent apoptosis, and *MLH1,* a gene identified previously as required for p53-dependent tumor suppression in a B cell lymphoma model,[44] were also identified as mediators of Nutlin sensitivity in our genetic screen (Figures 2C and S2D).

To further prioritize this candidate gene list, we evaluated their behavior in the GDSC dataset. Among the 54 candidates, expression of only a small subset was associated with Nutlin sensitivity across the hundreds of cell lines in this dataset (Figures 2D and 2E). In addition to *TP53, BBC3,* and *MLH1*, the top 10 screen hits associated with Nutlin sensitivity were *XYLT1, C12orf43, GPATCH8, EPHA3, FMNL3, CIC,* and *FAM193A.* In a complementary analysis, we evaluated the behavior of the 54 screen hits in the DepMap Project dataset.[45] The DepMap project completed genome-wide CRISPR genetic screens on 808 cell lines (dataset 20Q4), enabling generation of "gene effect" scores assessing the impact of thousands of genes on cell fitness and viability. In this dataset, when analyzing only *TP53* wild-type cell lines (n = 261), inactivation of *TP53* leads to increased cell viability and positive gene effect scores, as expected for a tumor suppressor, while inactivation of the p53 repressor genes *MDM2, MDM4,* and *PPM1D* (encoding WIP1) has the opposite behavior, leading to negative gene effects, as expected for oncogenes (Figure S2E). Additionally, the DepMap dataset enables identification of genetic interactions, whereby genes with agonistic functions show positive codependencies, and antagonists display negative codependencies. Reassuringly, when all genes analyzed in the DepMap dataset are ranked by their codependency with *TP53,* key cofactors and effectors of the p53 pathway show positive codependencies, as illustrated by *TP53BP1* and *CDKN1A* (encoding p21) (Figures 2F and S2F). In contrast, negative regulators of *TP53,* such as *MDM2* and *PPM1D,* show strong negative codependencies (Figures 2F and S2F; Table S4). Importantly, the DepMap dataset revealed that the candidate gene *FAM193A* displays the strongest positive codependency with *TP53* among the screen hits (Figures 2F and 2G). In fact, *FAM193A* was one of 2 screen hits associated with sensitivity to Nutlin and strong *TP53* genetic codependency (Figures 2H and S2G). Furthermore, when we calculated genetic codependencies of the *FAM193A* gene with all genes in *TP53* wild-type (WT) cell lines, *TP53* ranked as the top positively correlated gene (Figure 2I, Table S4). Other prominent highly-ranked positive codependencies for *FAM193A* include the DNA damage sensor *TP53BP1* and the p53 target gene *ZMAT3* (Figures 2I, 2J, and S2H). In contrast, top negative codependencies with *FAM193A* are the p53 repressors *PPM1D, MDM2,* and *MDM4* (Figures 2I, 2J, and S2H).

Therefore, from this point forth, we focused our efforts on FAM193A, a factor with an unknown role within the p53 network.

FAM193A is a positive regulator of p53 activity

Next, we decided to validate the effect of FAM193A on the cellular phenotype upon p53 activation. In our screen, two different sgRNAs targeting *FAM193A* scored as significantly enriched upon Nutlin treatment (Figures S3A and S3B). To confirm the screen results, we created multiple single-cell CHP212 clones lacking FAM193A expression via CRISPR

editing, with three single sgRNAs targeting two different exons and a pair of sgRNAs targeting 2 exons simultaneously, and compared them with single-cell clones carrying non-targeting sgRNAs (Figures S3A and S3C). On average, these single-cell clones showed significantly impaired responses to Nutlin, as seen by cell cycle profiling at multiple doses of Nutlin (Figures S3D–S3F). Substantial weakening of the cellular response to Nutlin in cells depleted of FAM193A is illustrated by comparison with clones lacking CDKN1A/p21, a key mediator of p53-induced cell-cycle arrest (Figures 3A, 3B, and S3D). The impairment of Nutlin action in *FAM193A* KO clones was also evident in an MTT assays of metabolic activity (Figure S3G) and in cell proliferation assays (Figure S3H). Furthermore, a similar trend was observed in *FAM193A* knockout (KO) cells treated with the genotoxic chemotherapeutic drug 5-fluorouracil (5-FU), which exerts p53-dependent and -independent effects (Figures S3I and S3J). We then analyzed the impact of FAM193A depletion on p53 stabilization and expression of key components of the p53 network. Remarkably, *FAM193A* KO cells showed decreased accumulation of total p53 protein upon Nutlin treatment, concurrent with decreased induction of the canonical p53 targets p21, TP53I3, PUMA, BAX, and MDM2 (Figure 3C). Notably, expression of MDM4 was elevated in FAM193A-depleted cells in DMSO- and Nutlin-treated cells (Figure 3C). Furthermore, when we generated KO single cell clones of *FAM193A* in two more cell lines of different origins, 94T778 (liposarcoma) and A549 (lung carcinoma), loss of FAM193A consistently led to an increase in MDM4 levels along with reduced expression of key p53 targets, with some variations across cell lines, such as lower MDM2 and PUMA expression in 94T778 cells and lower p21 expression in A549 cells (Figure S3K).

We then analyzed the impact of FAM193A depletion by transcriptome analysis via RNA sequencing (RNA-seq) in CHP212 cells treated with Nutlin or vehicle (DMSO) for 12 h. Nutlin treatment caused vast changes in gene expression in CHP212 cells, leading to upregulation of 641 mRNAs and downregulation of 332 mRNAs (|log 2 fold change [log2FC]| > 1.5, 5% false discovery rate [FDR]) (Figure 3D; Table S5). Notably, *FAM193A* KO cells showed fewer gene expression changes upon Nutlin treatment, whereby only 289 induced and 39 downregulated genes were identified using the same statistical cutoff (Figures 3D and S3L). When differentially expressed genes (DEGs) are ranked by decreasing FC in WT cells, it becomes apparent that, while the overall transcriptional response to Nutlin is qualitatively conserved in *FAM193A* KO cells, the quantitative effects of the drug are clearly diminished (Figure 3E), as would be expected from lesser p53 stabilization concurrent with elevated levels of MDM4. The decreased transcriptional output is also obvious when focusing on a curated list of core p53 target genes[6] because induction of most of them is clearly lower in *FAM193A* KO cells compared with the WT (Figure 3F). Besides a lower FC induction of core p53 target genes, their absolute expression levels in *FAM193A* KO cells are lower than in control cells (Figure 3G). To further investigate the mechanism of p53 transcriptional activity suppression observed in *FAM193A* KO cells, we performed p53 chromatin immunoprecipitation (ChIP) followed by quantitative PCR of select core p53 target genes. We found that changes in p53 promoter occupancy elicited by FAM193A depletion are gene specific, suggesting that suppression of p53-mediated transcription in *FAM193A* KO cells could be due to a combination of

reduced p53 chromatin binding (as expected from lower total p53 levels) and/or reduced p53 transactivation (as expected from higher levels of MDM4) (Figure S3M).

Altogether, these results demonstrate the FAM193A is a positive regulator of p53 activity.

FAM193A binds to the RING domain of MDM4

Next, we focused on the observed upregulation of MDM4 in FAM193A-depleted cells. Noteworthy, overexpression of MDM4 attenuates while knockdown of MDM4 exacerbates the response to Nutlin in multiple settings.[32,46,42] RNA-seq analysis (Table S5) followed by RT-PCR validation (Figure S4A) showed no changes in *MDM4* or *TP53* mRNA expression in *FAM193A* KO cells, suggesting that FAM193A acts through post-transcriptional mechanisms. Interestingly, review of the Biological General Repository for Interaction Datasets (BioGrid)[47] and the IntAct Molecular Interaction Database[48] suggested a physical interaction between FAM193A and MDM4 that was detected with affinity purification-mass spectrometry in the BioPlex 2.0[49] and BioPlex 3.0[50] project datasets (Figure S4B). Immunoprecipitation of FLAG-tagged FAM193A or endogenous MDM4 revealed that FAM193A and MDM4 indeed form a complex in CHP212 cells (Figures 4A and 4B). Because of lack of a FAM193A antibody suitable for immunoprecipitation, we used exogenously expressed FLAG-tagged FAM193A. Importantly, the expression level of FLAG-FAM193A was similar to that of the endogenous protein (Figure S4C). Identification of FLAG-FAM193A/MDM4 complex formation prompted us to investigate whether FAM193A also interacts with MDM2. We performed a Halo-FAM193A pull-down in unstimulated and Nutlin-treated cells and found that MDM4 and MDM2 co-precipitate with FAM193A, suggesting that all three proteins form a ternary complex (Figure 4C). Next, given that FAM193A interacts with MDM4 and that FAM193A depletion deregulates p53, MDM4, and MDM2 protein levels, we evaluated whether formation of the p53/MDM2/MDM4 complex is affected by FAM193A ablation. Co-immunoprecipitation experiments showed that MDM2 and MDM4 interact with each other and with p53 regardless of the presence of FAM193A, but the composition of the complex reflects the changes in protein expression caused by FAM193A depletion (Figures 4D and 4E).

To identify which functional domain of MDM4 may interact with FAM193A, we employed a uniquely tagged MDM4 construct, named MDM4c3, which has individual domains labeled with FLAG, myc, or hemagglutinin (HA) tags, and the domains are flanked with PreScission (PreS) protease cleavage sites (Figure 4F).[52] Through a combination of pull-down and protein digestion to remove non-captured domains, MDM4c3 enables a validated approach for identification of MDM4 interaction domains.[52,53] Overexpression of MDM4 along with a Halo-FAM193A construct followed by Halo-tag pull-down and PreS protease digest revealed that FAM193A binds to the RING domain of MDM4 (Figure 4G), a domain critical for MDM4 homodimerization and heterodimerization with MDM2. We then tested the impact of two mutations in the MDM4 RING domain shown to be important for the MDM4-MDM2 interaction, a deletion of the last 8 amino acids of the MDM4 C terminus (ΔC) and the point mutant C463A,[54–56] on the interaction with FAM193A, which revealed that the ΔC mutant shows decreased interaction with FAM193A (Figure S4D). We then aimed to map the domain(s) of FAM193A involved in the interaction with MDM4/

MDM2. Toward this end, we cloned five different fragments of the FAM193A polypeptide corresponding to major potential structural domains identified by MobiDB software (1,515 amino acids, NM_001366318.2)[51] (Figure 4H). We expressed the Halo-tagged versions of these fragments and completed Halo pull-down experiments, which demonstrated that MDM4 and MDM2 interact primarily with the with the N-terminal domain and, to a lesser degree, with the C-terminal domain of FAM193A (Figure 4I).

Furthermore, through subcellular fractionation of CHP212, HCT116, and H4 cells, and via immunofluorescent detection of 3×FLAG-FAM193A in H4 cells, we observed that FAM193A localizes in the nuclear and cytoplasmic compartments together with MDM4 and MDM2 (Figures S4E and S4F). The subcellular localization of FAM193A is very heterogeneous from cell to cell and can range from mostly cytoplasmic to almost exclusively nuclear localization; often, FAM193Acan be found in the perinuclear region. Importantly, the subcellular localization of p53 and MDM4 does not change significantly in FAM193A-depleted cells (Figure S4G). Overall, these findings show that FAM193A interacts with and is present in the same subcellular compartments as MDM4 and MDM2.

Last, we decided to investigate the impact of FAM193A depletion on MDM4 protein stability and its ubiquitination status. After treatment with cycloheximide (CHX) to inhibit global mRNA translation, we observed that MDM4 half-life in CHP212 cells extends beyond 16 h, rendering quantification of MDM4 half-life in this system imprecise because of CHX toxicity at later time points (Figure S4H). The slow turnover of MDM4 in CHP212 is further underscored by the lack of MDM4 accumulation upon proteasome inhibition with carfilzomib (Figure S4I). Hence, we performed a CHX chase assay in A549 control and *FAM193A* KO cells and found a 50% increase in MDM4 protein half-life (from 6.6 to 9.9 h) in cells depleted of FAM193A (Figures S4J and S4K).

Hence, given that *FAM193A* KO leads to an increase in MDM4 levels, and that MDM4 upregulation is known to suppress the response to Nutlin,[32,46,42] these results indicate that FAM193A is a positive regulator of the p53 network likely acting by increasing MDM4 turnover (Figure 4J).

Increased *FAM193A* mRNA levels correlate with better survival in specific cancer types

To further investigate the potential role of FAM193A in carcinogenesis, we analyzed a comprehensive gene expression dataset with unified data from The Cancer Genome Atlas (TCGA) program and the Genotype-Tissue Expression (GTEx) project comparing tumor samples with corresponding healthy tissues.[57] This analysis revealed that *FAM193A* mRNA expression is mostly higher in healthy control tissues compared with tumor samples, with a few exceptions (Figures 5A and 5B). Analysis of *FAM193A* mutations and copy number variations (CNVs) in *TP53* WT tumors in the TCGA dataset[58] revealed a high frequency of *FAM193A* mutations in select tumor types, such as colorectal adenocarcinoma (COAD), uterine corpus endometrial carcinoma (UCEC), bladder urothelial carcinoma (BLCA), skin cutaneous melanoma (SKCM), and stomach adenocarcinoma (STAD) (Figure 5C). Furthermore, the distribution of missense and nonsense mutations along the *FAM193A* gene is not random, which is manifested by a high incidence of mutations at specific sites (such as mutations leading to changes at V522, L964, and M1124) and accumulation of mutations at

certain stretches of *FAM193A* sequence, such as the fragment we annotated as #4 and which we found to interact preferentially with MDM2 (Figures S5A and 4I). Notably, very few mutations were found in the region encoding the very N terminus of FAM193A, which we found to interact with MDM4 and MDM2. Additionally, analysis of *TP53* WT tumors in the TCGA Pan-Cancer Clinical Data[59] showed that, in 6 cancer types (of 33 analyzed), higher expression of *FAM193A* mRNA is a predictor of better overall patient survival (BLCA, head and neck squamous cell carcinoma [HNSC], UCEC, lung squamous cell carcinoma [LUSC], pancreatic adeno-carcinoma [PAAD], and thyroid carcinoma [THCA]) (Figures 5D and 5E). In contrast, higher expression of *FAM193A* was only associated with lower overall survival in one cancer type, pheochromocytoma/paraganglioma (PCPG) (Figure S5B), a very rare and primarily benign tumor type.[60]

DISCUSSION

Since its discovery over 40 years ago,[61–63] the importance of p53 in tumor biology remains unabated. Given that functional p53 promotes the efficacy of several genotoxic therapies,[64] targeted inhibition of the p53-MDM2/4 interaction with non-genotoxic agents has been the focus of much research and development activities. Unfortunately, these efforts have not yielded the expected results in clinical trials, justifying the development of biomarkers of efficacy and combinatorial therapies. Our analysis of the GDSC dataset, arguably the largest available dataset for analysis of Nutlin sensitivity, revealed that the response to this compound is associated with high basal transcriptional output within the p53 network before drug treatment. This finding agrees with previous efforts identifying gene signatures that predict sensitivity to structurally diverse MDM2 inhibitors.[41,40,65] Therefore, identification of factors modulating the transcriptional output of the p53 network could lead to improved use of MDM2/4 inhibitors.

To identify positive regulators p53 function upon MDM2 inhibition, we employed a multi-omics approach involving a CRISPR screen in a highly Nutlin-sensitive cell line and matched Nutlin sensitivity and gene expression data available from the GDSC and genetic interaction data from the DepMap project. Confidence in the results of our screen is provided by the fact that the top hits included not only *TP53* itself but also known effectors of the p53 network, such as *BBC3,* a p53 target gene encoding the pro-apoptotic protein PUMA,[35,36] and *MLH1,* a mediator of p53-dependent tumor suppression in a mouse model of B cell lymphoma.[44] Furthermore, many of the screen hits, such as G-patch domain-containing 8 (*GPATCH8*), hypoxia-inducible factor 1 subunit alpha inhibitor (*HIF1AN*), and A-kinase anchoring protein 8-like (*AKAP8L*) have been found to interact with p53,[66–68] but their roles in control of p53 function are unknown. GPATCH8 may be involved in pre-mRNA processing.[69] AKAP8L is a nuclear protein that binds to the C terminus of RNA helicase A and acts as a transcriptional coactivator;[70,71] it is also involved in initiation of DNA replication[72] and positively modulates mTORC1 activity.[73] HIF1AN1, a hydroxylase, has been found to modulate the expression of p63α, a member of the p53 family,[74] but a direct role in p53 regulation is not clear.[75] To prioritize our investigation of screen hits, we integrated the screen results with the Nutlin sensitivity data and *TP53* codependency data, which pointed to FAM193A as a widespread regulator of p53 activity. Notably, *FAM193A*

is part of the 175-gene signature that predicts sensitivity to the structurally diverse MDM2 inhibitor DS-3032b.[40]

Encoded by a gene in the Huntington's disease locus, very little is known about the molecular function of the FAM193A protein. The few published studies primarily link FAM193A to neurological disorders such as Wolf-Hirschhorn syndrome[76] or autism[77] and to cancer-related osteonecrosis of the jaw and osteoporosis.[78] A region within 200 bp of a transcription start site for *FAM193A* was found to be hypomethylated in the dorsolateral prefrontal cortex in humans compared with chimpanzees and macaques.[79] Last, autoantibodies targeting FAM193A are associated with neurological disease in patients with cerebral ischemia.[80] Our study describes a molecular and cellular role of FAM193A in control of MDM4 levels and modulation of the p53 transcriptional program. Noteworthy, previous studies clearly demonstrated that expression levels of MDM4 regulate the response to Nutlin in multiple cell types.[32,46,42] Depletion of FAM193A leads to reduced transcriptional output upon p53 activation and subsequent dampening of the downstream cellular response. Although, our results indicate that FAM193A regulates MDM4 protein levels at the post-translational level through modulation of its half-life, the exact underlying mechanism driving this effect is unclear, especially in cells with a very long half-life of MDM4. Proteomics studies suggests that FAM193A forms a complex with four subunits of the carbon catabolite repression-negative on TATA-less (CCR4-NOT) complex,[81] a transcriptional regulatory complex that also acts as a mRNA deadenylase repressing translation.[82,83] FAM193Aisalso predicted to interact with cytoplasmic polyadenylation element binding protein 4 (CPEB4), a p53 target gene involved in control of polyadenylation,[81,84–86] and with the cap binding complex-dependent translation initiation factor (CTIF), a component of the CBP80 translation initiation complex.[81,87] Hence, the exact mechanism of MDM4 upregulation following FAM193A depletion may involve post-transcriptional events worthy of future investigations.

We discovered that FAM193A interacts with the RING domain of MDM4. Mutations in the RING domain of murine *Mdm4* are as detrimental as KO of *Mdm4,* with embryonic lethality occurring at embryonic day 9.5[14,88]. The RING domain of MDM4, unlike that of MDM2, does not possess an intrinsic E3 ubiquitin ligase activity critical for targeting p53 for proteasomal degradation. However, the MDM4 RING domain is crucial for stabilizing MDM2 through MDM2-MDM4 heterodimerization and, thus, aiding p53 ubiquitination.[55,56,88,89] Heterodimerization between MDM4 and MDM2 is critical for p53 inhibition *in vivo,* as demonstrated by transgenic mouse models harboring MDM4 RING domain deletions or mutations, which cause p53-mediated early embryonic lethality despite MDM4 being still able to bind to p53.[54,90]

Although our data indicate that FAM193A controls the dynamics of the MDM4/MDM2/p53 complex primarily through modulation of levels of the individual components of this complex, it is possible that FAM193A binding to the RING domain of MDM4 may interfere with the activity of the MDM2-MDM4 heterodimer, leading to higher p53 protein expression and activity.

Compared with the number of *TP53* mutations/deletions, the frequency of *FAM193A* gene alterations in cancers is much lower (~2.3%). However, the *FAM193A* alteration rate is comparable with that of genes encoding established modulators of the p53 network, such *MDM2, MDM4, PPM1D, CDKN1A, BAX,* or *BBC3,* which range from 0.7%–4% (source: CBioPortal query of the TCGA Pan-Cancer Atlas Studies). Our analyses point to *FAM193A* as a potential tumor suppressor gene in three major cancer types, BLCA, UCEC, and LUSC, a notion that will require further experimental evaluation. All three tumor types exhibit lower *FAM193A* mRNA expression in cancer samples compared with healthy tissue, a high number (>5%) of *FAM193A* mutations/deletions in *TP53* WT tumors, and better survival of patients carrying tumors with high *FAM193A* mRNA expression. In LUSC, a cancer with an overall very high mutational rate, *TP53* is mutated in over 80% of tumors,[91] and p53 reactivation may not be a feasible therapeutic approach for most LUSC patients. In bladder cancer, while *TP53* is mutated/deleted in 49% of muscle-invasive cancers, it is less frequently altered in superficial tumors, suggesting that p53 suppression promotes tumor invasion.[92–94] In UCEC, *TP53* mutations occur primarily in one endometrial cancer subtype, copy-number high (serous-like), which is characterized by the lowest progression-free survival of all four UCEC subtypes and accounts for approximately a quarter of the cases.[95] Therefore, p53 reactivation in BLCA or UCEC tumors expressing high levels of FAM193A should be considered as a potential therapeutic approach, especially during early stages of disease.

Overall, our results describe the identification of FAM193A as a widespread positive regulator of p53 activity, with clear roles in promoting the therapeutic efficacy of MDM2 inhibition, which justifies further investigations into its potential roles as a candidate tumor suppressor gene in several major tumor types.

Limitations of the study

This study identifies FAM193A as a regulator of p53 activity in the context of cancer cell line cultures through our own experiments and analysis of public datasets generated from cancer cell lines. However, the role of FAM193A in control of p53 activity *in vivo* has not been defined and will require further investigation, including in animal models. Another limitation of this study is that it focuses mostly on the cellular response to p53 activation upon non-genotoxic inhibition of its repressor MDM2 without fully defining the role of FAM193A in many other scenarios leading to p53 activation via stress-induced signaling cascades.

STAR★METHODS

RESOURCE AVAILABILITY

Lead contact—Further information and requests for resources and reagents should be directed to and will be fulfilled by the lead contact, Dr. Joaquin Espinosa (joaquin.espinosa@cuanschutz.edu).

Materials availability—All materials developed for this project, including plasmids and cell lines, will be made available upon request to the lead contact upon completion of material transfer agreements when appropriate.

Data and code availability

- RNA-seq data have been deposited in the Gene Expression Omnibus under accession number Gene Expression Omnibus: GSE189133. CRISPR screen has been deposited at the Gene Expression Omnibus under accession number Gene Expression Omnibus: GSE189132. All data are publicly available as of the date of publication. DOIs are listed in the key resources table.
- This paper does not report original code.
- Any additional information required to reanalyze the data reported in this paper is available from the lead contact upon request.

EXPERIMENTAL MODEL AND SUBJECT DETAILS

Cell lines—All cell lines were maintained at 37°C, 5.0% CO_2 in Gibco cell culture media: CHP212 (derived from male human neuroblastoma) in DMEM:F12 (1:1); 94T778 (derived from female human liposarcoma tissue) in DMEM:F12 (1:1); SJSA1 (derived from male human osteosarcoma) in RPMI-1640; A549 (derived from male human lung adenocarcinoma) in RPMI-1640; HEK293FT (derived from female human embryonic kidney tissue) in DMEM; MCF7 (derived from female human breast carcinoma metastasis) in DMEM; H4 (derived from male astrocytoma sample) in DMEM; HCT116 (derived from male human colorectal carcinoma tissue) in McCoy's 5A. Cell lines identities were confirmed by STR analysis at the CU Anschutz Cell Technologies Shared Resource laboratory. Each medium was supplemented with 10% FBS (Peak Serum), except for 94T778 medium, which was supplemented with 10% EquaFetal (Atlas Biologicals), and 100 units/mL of penicillin, 100 μg/mL of streptomycin, and 250 ng/mL of amphotericin B (Gibco). Matching cultivation conditions were used for maintaining derived lineages: CHP212 stably transduced with 3xFLAG-FAM193A, HCT116 transiently transfected with Halo-FAM193A (full length and fragments 1–5) and MDM4-V5, and HEK293FT transiently transfected with Halo-FAM193A MDM4c3 (WT, deltaC, and C463A variants).

METHOD DETAILS

Analysis of GDSC dataset—Drug sensitivity information, which included measurements of Nutlin-3a (−) responsiveness, was obtained from the Genomics of Drug Sensitivity in Cancer (GDSC) database (www.cancerrxgene.org).[37] The drug sensitivity dataset used in the analysis was part of the release-7.0 (v17.3_fitted_dose_response). Gene expression data was also obtained from GDSC (RMA normalized expression data of dataset E-MTAB-3610[96]). Genomic alteration information (*TP53* mutations and *MDM2* amplification) was acquired from cBioPortal database through querying the Cancer Cell Line Encyclopedia dataset[97] which includes full profiles of 881 cell lines. Sensitivity to Nutlin was analyzed only in cells with known *TP53* mutational status (unprofiled cell lines were excluded from the analysis). Comparison of Nutlin IC_{50} values was performed with unpaired two-samples Wilcoxon test. Correlations between robust multi-array analysis

(RMA) algorithm normalized gene expression and Nutlin ln(IC_{50}) values were calculated for *TP53* WT cell lines only regardless of *MDM2* amplification status using the Spearman method. p-values were adjusted with the Benjamini-Hochberg procedure.

Gene set enrichment analysis—Gene set enrichment analysis was performed using the GSEA software (v 4.1.0; Broad Institute). The full list of 17,419 genes ranked by correlation values of Nutlin sensitivity vs. gene expression levels was compared to lists of: (1) core p53 target genes,[6] (2) genes predicting sensitivity to compound NVP-CFC218,[41] and (3) genes predicting sensitivity to compound DS3032b.[40] The enrichment analysis used a classic Kolmogorov-Smirnov scoring scheme with 1000 permutations and the enrichment scores were calculated with weighted statistics.[98]

Ingenuity pathway analysis—Upstream regulator prediction using Ingenuity Pathway Analysis (IPA) was performed for the top 100, 250, 500, and 1000 genes negatively correlated with Nutlin sensitivity. To simplify the interpretation of the results the input R values have been multiplied by −1. Results of the IPA upstream regulator analysis have been filtered to include only transcriptional regulators of the top 100 anti-correlated genes with a p value of overlap smaller than 0.05 and for which *Z* score has been calculated.

Nutlin treatment—Cells were treated with Nutlin at concentrations indicated in applicable Method's section, figure legends and figure panels. Nutlin stock solution was prepared as a 10 μM Nutlin-3R (racemic mixture of 3a and 3b isoforms) in DMSO. Final concentrations are presented as concentrations of the MDM2-inhibiting isoform Nutlin-3a.

CRISPR screen in CHP212 cells—Lentiviral particles of Human GeCKO v2 Library A and B[43,99] were prepared by the Functional Genomics Core at the University of Colorado Anschutz as described previously.[100] CHP212 cells were plated onto two 15 cm plates at 12×10^6 cells per plate and transduced separately with GeCKO v2 Library A and Library B virus by adding viral supernatant together with 8 μg/mL Polybrene to cells. Viral titer was tested in parallel to ensure that virus added was < MOI = 1. Virus was removed after 16 h and replaced with fresh DMEM:F12 media. Cells were selected in 2.5 μg/mL of Puromycin starting on day 3 after transduction. Following the puromycin selection Library A and Library B cells were combined and cultured for 10 days to allow for dropout of essential genes. Next, 36×10^6 library-containing cells were plated on three 15 cm plates at 12×10^6 cells per plate and treated the next day with DMSO (vehicle control) or 10 μM Nutlin, three plates for each condition. At 48 h, DMSO-treated cells were harvested for gDNA extraction (see below) and Nutlin treatment was removed and replaced with regular growth media to allow for recovery of the cell culture. Once cells reached about 90% confluency, each Nutlin replicate was replated in anew 15 cm plate for a second round of 10 μM Nutlin treatment. After 48 h, Nutlin-3a-containing media was removed and again replaced with regular growth media. Cells were allowed to repopulate the plate in the recovery time and were then harvested for gDNA extraction using the DNeasy Blood and Tissue kit (Qiagen). PCRand library preparation of GeCKO v2 gRNA cassettes were accomplished as described previously,[100] with the exceptions noted here. In brief, we used a nested PCR to build barcoded sgRNA cassette libraries suitable for Illumina sequencing for

each replicate. To achieve 10-fold representation of the library and to maintain appropriate DNA concentrations for PCR, we ran 16 separate 50 μL PCR reactions using 500 ng template DNA to generate 8 μg of PCR product DNA per sample (primers: PCR1-fwd and PCR1-rev). PCR1 reactions were pooled, purified, and 50 ng were used for a second PCR, where barcodes and sequencing primers were attached to each cassette. PCR2 was accomplished with 10 μL of 5x Phusion HF buffer (ThermoFisher Scientific), 1 μL dNTPs (10 mM), 2 μL FWD and REV primer (10 μM), 1 μL Phusion polymerase (ThermoFisher Scientific) and 15 μL of nuclease-free water in 50 μL total reaction (primers: PCR2-fwd and PCR2-rev1-4 barcoded primers). PCR conditions for second PCR were: 1 cycle at 98°C for 5 min, 2 cycles of 98°C for 30 s, 55°C for 30 s, 72°C for 30 s, then 6 cycles of 98°C for 30 s, 65°C for 30 s, and 72°C for 30 s, and a final extension at 72°C for 5 min. PCR products were purified and assessed on the 2100 Bioanalyzer (Agilent) for quality prior to submission to the University of Colorado Cancer Center Genomics and Microarray Core Facility for Illumina sequencing.

CRISPR screen data analysis—CRISPR data analysis was carried out as described previously.[100] Briefly, signal processing, base-calling, and quality scoring was carried out automatically by the HiSeq 2500 Real-Time Analysis software (Illumina). Conversion to fastq format was performed with bcl2fastq (v1.8.4, Illumina). Next, samples were demultiplexed, allowing 2 mismatches, using fastx_barcode_splitter from the fastx_toolkit (v0.0.13.2). Sequence data quality was assessed with FASTQC (v0.11.2). Next, sequences were trimmed using fastx_trimmer from the fastx_toolkit (v0.0.13.2), with the following options: -Q33 -f 43 -L 62, which kept only the section of each read corresponding to the unique sgRNA sequences (positions 43–62 inclusive). Bases with qual ≥ 10 were removed with fastx_quality_filter from thefastx_toolkit (v0.0.13.2; options: -Q33 -q 10 -p 94). Trimmed and filtered sequences were mapped with Bowtie2 (v2.2.3; options –phred33 –end-to-end –very-sensitive) and a reference index was generated for Bowtie2 using only the unique sgRNA sequences from the Human GeCKO v2 library annotation available from https://media.addgene.org/cms/filer_public/7d/87/7d87eaa7-e940-41bf-bf2f-47b43c7ab905/zhang_human_geckov2_grna_sequences.zip[43,99]). Read counts for each sgRNA were calculated using SAMtools idxstat (v0.1.19). Top Nutlin-enriched screen hits were filtered based on the following criteria: (1) $\log_2$(counts per million) $\gneqq$ 3, (2) $\log_2$(fold change (Nutlin/DMSO)) $\gneqq$ 2, and (3) gene occurrence $\gneqq$ 2.

Analysis of the DepMap dataset—Gene effect data (“Achilles_gene_effect”) and gene mutation data (“CCLE_mutations”) have been downloaded from the DepMap database (release 20Q4). Only cell lines that have been profiled in the “CCLE_mutations” dataset have been included in the analysis. Cell lines with silent mutations of *TP53* were considered as WT. Out of 1749 cell lines, 1084 had genetic alterations in *TP53* and were excluded from downstream analysis. Out of the 665 remaining cell lines with WT *TP53,* 261 cell lines were profiled in the gene effect dataset. Gene codependencies were calculated as Spearman correlations between gene effects for 18,119 genes. p-values were adjusted with the Benjamini-Hochberg procedure.

Generation of *FAM193A* and *CDKN1A* knockout cells—Individual CRISPR-edited cell lines were generated by transfection with pSpCas9(BB)-2A-GFP (PX458), a gift from the Feng Zhang laboratory (Addgene plasmid #48138),[101] encoding GeCKO library sgRNAs targeting *FAM193A* (GeCKO sgRNAs HGLibA_16363, HGLibA_16364, or HGLibB_16341) or control non-targeting sgRNA (GeCKO sgRNA HGLibA_64384/ HGLibB_57029). sgRNAs were cloned into the BbsI site of pX458 vector as described previously.[101] Next, sgRNA containing PX458 plasmids were transiently transfected into CHP212 cells (plated at 3×10^6 cells/10 cm dish and 5 μg of plasmid) using Lipofectamine 3000 (ThermoFisher Scientific). Media was changed next day, and on day 2 post-transfection cells were sorted for positive GFP expression by the University of Colorado Cancer Center Flow Cytometry Core. Cells were sorted into 96-well plates containing 1:1-fresh:pre-conditioned growth medium at 1 cell/well. Single-cell clones were expanded and screened for lack of FAM193A expression by Western blot (using antibody Abcam 122,832). The same single-cell clone *FAM193A* KO strategy was used to generate A549 and 97T778 using sgRNA vector pSpCas9(BB)-2A-GFP (PX458)-HGLibA_16364. Additionally, the clone used for RNA-seq experiments (Fam21) was validated for homozygous *FAM193A* gene deletion/edits by: PCR amplifying with Phusion High Fidelity DNA Polymerase (ThermoFisher Scientific) the region surrounding the edit site HGLibA_16364 (primers: FAM193A_cval_FWD_2 and FAM193A_cval_REV_2), A-tailing of PCR products, cloning PCR products into pCR4-TOPO-TA (ThermoFisher Scientific), and sequencing. CHP212 *CDKN1A* KO and additional *FAM193A* KO single-cell clones were generated with a dual sgRNA-targeting strategy through nucleofection of two gRNAs complexed with Alt-R S.p. Cas9 Nuclease V3 (Integrated DNA Technologies). gRNAs were produced through annealing of synthetic crRNAs (Hs.Cas9.CDKN1A.1.AA and Hs.Cas9.CDKN1A.1.AD; or Hs.Cas9.FAM193A.1.AB and Hs.Cas9.FAM193A.1.AC) with the universal Alt-R CRISPR-Cas9 tracrRNA. Next, sgRNAs were complexed with Cas9-NLS and then delivered by nucleofection into CHP212 cells using Lonza 4-D Nucleofector (pulse code CA-168) and SF Cell Line 4D-NucleofectorX Kit solutions. Following recovery, single cell clones were isolated and screened by PCR for edits using the following primers pairs: FAM193A-F/FAM193A-R and FAM193A-F2/FAM193A-R2 (for *FAM193A* CRISPR edits) or CDKN1A-F/CDKN1A-R and CDKN1A-F2/CDKN1A-R2 (for *CDKN1A* CRISPR edits). For gRNA and primer sequences see key resources table.

Generation of cell lines expressing 3xFLAG-FAM193A—The CHP212 and H4 TetR+3xFLAG-FAM193Acell lines have been generated through stable integration of lentiviral constructs. Lentivirus was produced as follows: $6{\times}10^6$ HEK293FT cells were plated on 15 cm cell culture dishes. After 24 h, transfection mix was prepared by combining in 500 μLof Opti-MEM (Gibco) with: 6.8 μg psPAX2 DNA, 3.4 μg pMD2.G, 3.4 μg pLenti-CMV/TO-3xFLAG-FAM193A, and 3.4 μg pLenti-CMV-TetR-Blast. DNA-PEI complexes were formed through addition of with 34 μL 1 mg/mL polyethyleneimine (PEI) (final ratio of DNA:PEI was 1:2 – PEI batch optimized). DNA-PEI mix was incubated at room temperature for 15 min. HEK293FT cells were replenished with fresh growth medium and DNA-PEI was added dropwise and mixed. Cells were incubated for 18 h with DNA-PEI mix before replenishing with fresh growth medium. Growth medium with lentiviral particles were collected 48 h post-transfection and filtered through 0.45 μm cellulose acetate filter.

Destination cells were plated at 6×10^6 on 15 cm plates and transduced with lentiviral filtrate diluted in fresh medium with polybrene (8 μg/mL final). 24 h post-transduction, cells were replenished with fresh medium and following another 24 h, puromycin and blasticidin were added to the medium for stable cell line selection (2.5 μg/mL final concentration of each selection antibiotics).

RNA-seq—Two independent biological replicates of CHP212 WT and *FAM193A* KO (Fam21 clone – fully sequence verified) cells were treated for 12 h with either 0.2% DMSO or 10 μM Nutlin. Total RNA was extracted using TRI-reagent (ThermoFisher Scientific) according to manufacturer's protocol. RNA quality was assessed using the 2100 Bioanalyzer and RNA 6000 PICO kit (Agilent). Samples submitted had an RNA integrity number greater than 8. RNA samples were submitted to Novogene for strand-specific library preparation and paired end reads on the Illumina HiSeq4000 platform. Signal processing, base-calling, and quality scoring was carried out automatically by the HiSeq 4000 RTA software (Illumina). Demultiplexing and conversion to FASTQ format was carried out using bcl2fastq (Illumina). Fastqc (v0.11.5) was used to assess sequence data quality. Fastq files from 2 separate lanes were merged for each sample to obtain sufficient read depth. Low quality bases (Q < 10) were trimmed from the 3' end of reads and short reads (<30 nt after trimming) and adaptor sequences were removed using the fastq-mcf (v1.05) tool from EAutils. Following fastq-mcf, sequence data quality assessed again with fastqc (v0.11.5). FastQ Screen (v0.9.1) was used to check for common sequencing contaminants. Alignment to the Human reference genome (GRCh37/hg19) was carried out using TopHat2 (v2.1.1, –b2-sensitive –keep-fasta-order –no-coverage-search –max-multihits 10 –library-type fr-firststrand) and Bowtie2 (v2.2.9.0) with the UCSC hg19 GTF annotation file provided in the iGenomes UCSC hg19 bundle. Read groups were created with Picard AddOrReplaceReadGroups version: 2.9.4. Aligned reads were then filtered to remove low quality mapped reads (MAPQ <10) using SAMtools (v1.5). Reads were coordinate-sorted and duplicates were marked using Picard SortSam and MarkDuplicates (v2.9.4). Alignment metrics were produced with Picard CollectAlignmentSummaryMetrics (v2.9.4). Quality assessment of final mapped reads was performed using RSeQC (v2.6.4). Raw gene-level count data was generated using HTSeq (v0.8.0) with the following options (−stranded = reverse −minaqual = 10 −type = exon −idattr = gene_id −mode = intersection-nonempty) using the GTF provided in the UCSC hg19-based iGenomes bundle. Differential gene expression data was generated with DESeq2 (v1.18.1) in R (v3.4.2).

Validation of RNA-seq was performed using Q-RT-PCR on RNA samples isolated from WT and *FAM193A* KO single cell clones (n = 4 and n = 5, respectively). For each line, cells were plated at $4.5*10^5$/well into 6-well plates and after 48 h treated with either 0.2% DMSO (vehicle control) or 10 μM Nutlin-3a for additional 12 h (technical duplicates for each cell line/treatment combination). RNA was isolated using TRIzol Reagent (ThermoFisher Scientific) according to manufacturer's instructions and cDNA was generated using High-Capacity cDNA kit (ThermoFisher Scientific) using 1 μg of RNA as template. qPCR reactions were set up using SYBR Select Master Mix for CFX (ThermoFisher Scientific) and primers provided in the key resources table. Amplicons were generated and quantified using a ViiA 7 instrument (Life Technologies).

Chromatin immunoprecipitation—Three biological replicates of CHP212 cells – nontargeting control and *FAM193A* KO cells – were plated onto eight 15 cm dishes at the density of $1.2*10^6$ cells per plate. After 48 h, cells were treated with either 0.2% DMSO or 10 μM Nutlin for 12 h (four 15 cm plates per treatment/replicate). At the time of collection, cultivation medium was replaced with 19 mL of 1% formaldehyde in 1x PBS and incubated at room temperature for 15 min. Formaldehyde crosslinking was terminated by adding 1 mLof 2.5 M glycine (125 mM final concentration). After 5 min incubation, cells were washed three times with ice-cold PBS and lysed with Szak's RIPA buffer (150 mM NaCl, 1% v/v NP40, 0.5% w/v sodium deoxycholate, 0.1% w/v SDS, 50 mM Tris pH 8.0, 5 mM EDTA, 0.65 mL per plate) with proteasome inhibitor cocktail (cOmplete Mini, Roche). Cell lysates were transferred to 15 mL conical tubes and sonicated on ice for 3 min and 45 s (15 cycles of 15 s on and 15 s off at 5W power output using VirTis Virsonic 600 sonicator). Lysates were centrifugated at 18,000 g for 15 min and supernatants were transferred to fresh tubes. Next, protein concentrations of the samples were analyzed by a BCA assay and lysates diluted to a final protein concentration of 1 mg/mL were dispensed to 1 mL aliquots. One aliquot per sample was pre-cleared with 20 μL of Protein G Dynabeads for 1 h at 4°C with rotational agitation. Next, lysates were incubated with either 0.5 μmg of p53 mouse monoclonal antibody (DO-1, OP43 Calbiochem) or control mouse IgG (sc-2025, Santa Cruz Biotechnology) and 40 μL of Protein G Dynabeads o/n at 4°C with rotational agitation. Next day beads were pelleted on a magnetic rack, washed two times with Szak's RIPA buffer, four times with Szak's wash buffer (100 mM TrisHCl pH 8.5, 500 mM LiCl, 1% v/v NP40,1% w/v deoxycholic acid), and again twice with Szak's RIPA buffer. Each wash was performed for 5 min at 4°C with rotational agitation. Protein complexes were eluted by adding of 100 μL of TE buffer and 200 μL 1.5xTalianidis Elution Buffer (70 mM Tris HCl pH 8.0,1 mM EDTA, 1.5% w/v SDS) and incubating for 10 min at 65°C. Eluate was collected in fresh tubes and combined with 5M NaCl solution to a final concentration of 200 mM and incubated for 5 h at 65°C. Following sample de-crosslinking, 20 μg of proteinase K was added to each tube. Samples were incubated at 45°C for 30 min and immunoprecipitated DNA was extracted with phenol:chloroform:isoamyl alcohol (25:24:1) followed by chloroform extraction. DNA was precipitated by adding 2 μLof GlycoBlue (ThermoFisher Scientific), 1/10 volume of 3M sodium acetate, and 2.5 volumes of 100% ethanol. Vortexed samples were incubated at −20°C and spun down at 18,000 g for 20 min. DNA pellets were washed with 70% ethanol, resuspended in 100 μL of 0.1 x TE, and analyzed by Q-PCR.

Annexin V assays—Cells were treated either with 0.2% DMSO or 10 μM Nutlin for 48 h in 6-well plates. Medium was collected and cells were washed with 1mL PBS per well. PBS used for the wash was pooled with the collected media. Next, cells were detached with 0.2 mL/well of 0.25% trypsin-EDTA for 2–5 min at 37°C and washed out of wells with collected medium-PBS mix and placed on ice until centrifugation for 5 min 100xg at 4C. Cells were re-suspended in 1 mL ice-cold PBS and spun down again and re-suspended in 80 μL Annexin V binding buffer (10 mM HEPES, 140 mM NaCl, and 2.5 mM $CaCl_2$, pH 7.4) before adding 20 μL Annexin V master mix (100:1:1/Annexin V binding buffer:Annexin V-FITC:1 mg/mL PI). Cells when there incubated at room temperature for 15 min and

placed on ice. FITC and PI fluorescence intensities were then measured with a BD Accuri C6 Flow Cytometer (BD Biosciences).

MTT metabolic activity assays—Single cell clones (5 non-targeting controls and 12 *FAM193A* KO lines) were plated into 96-well plates at $1.5*10^4$ cells per well in 0.1 mL/well. After 36 h, cells were treated with DMSO or 2.5 and 5 μM Nutlin and cell viability was measured at 24-h intervals. Thiazolyl blue tetrazolium bromide stock was prepared at 5 mg/mL in PBS. Stock solution was diluted then as a 2x working solution in cultivation medium and added to cells to a final concentration of 0.3 mg/mL. Cells were incubated at 37° for 2 h. Medium was then gently removed, formazan was extracted with 4 mM HCl 0.1% NP40 in isopropanol and quantified via absorbance measurements at 570 nm.

Cell proliferation assay—Single cells clones (5 non-targeting controls and 5 *FAM193A* KO lines) were plated into 12-well plates at $2.5*10^5$ cells/well. Cells were counted using a hematocytometer (eight 1 × 1 mm corner squares were counted per line) before dilution and plating. Following 24 h, cells were treated with either DMSO or 1.25 μM Nutlin (in duplicates) for 24 h. Following the treatment period, cells were detached by trypsinization and counted using a hematocytometer (eight 1 × 1 mm corner squares were counted per cell clone/treatment/technical replicate).

DNA content-based S phase quantification—Single cell clones (see figure legends for number of clones used in each experiment) were plated into 6-well plates at $2.5*10^5$ cells/well. After 48 h, cells were treated with either vehicle or 1.25 or 2.5 μM Nutlin (in duplicate) for 24 h. After treatment cells were detached via trypsinization and washed twice with PBS (between washes cells were centrifugated at 250 g for 5 min at room temperature). Next, cells were resuspended in 0.1 mL PBS and then fixed with 1 mL of 70% ethanol overnight at 4°C. Fixed cells were washed twice with 0.1% Triton X-100 in PBS, followed by overnight incubation in 10 μg/mL propidium iodide, 33 μg/mL RNase A. Next, samples were passed through a 23G needle and PI intensity was measured with BD Accuri C6 Flow Cytometer (BD Biosciences). Cell cycle analysis and downstream quantification of cells in S-phase was performed with FlowJo (v10.7.2). Cell cycle profiles were generated with FlowJo's Cell Cycle Analysis tool using the Dean-Jett-Fox univariate model.

Bromodeoxyuridine incorporation assays—CHP212 cells (3 single cell clone lines per each, nontargeting control and *FAM193A* KO) were plated at $4*10^5$ cells per well into 6-well plates. Following 48 h, cells were treated with either 0.05% DMSO or 1.25 or 2.5 μM Nutlin or 24, 47, or 97 μM 5-fluorouracil for 24 h. Bromodeoxyuridine (BrdU) solution was added to the cells at a final concentration of 10 μM for the last hour of the cultivation period. After the treatment, cells were detached via trypsinization and washed twice with PBS (250g 5 min spin-downs between washes). Next, cells were resuspended in 0.1 mL PBS and fixed by 1 mL of 70% ethanol. Cells were fixed overnight at 4°C, washed once with 0.1% Triton X-100 in PBS and incubated in 0.5% Triton X-100 in 2 M HCl at 37°C for 10 min. After the DNA denaturation step, cell suspensions were neutralized with 0.1 M NaB_4O_7 pH 8.5 for 10 min. Samples were washed once with 1% BSA-0.1% Triton X-100 in PBS and then incubated with a fresh aliquot of 1% BSA-0.1% Triton X-100 in PBS for

1 h at room temperature. Next, cells were incubated with agitation overnight at 4°C with anti-BrdU antibody and for 1 h at room temperature with goat anti-mouse IgG conjugated to Alexa Fluor 488. Lastly, nuclei were stained with 10 μg/mL propidium iodide and 40 μg/mL RNaseA in 0.1% Triton X-100 in PBS for 30 min at 37°C. BrdU/PI levels were measured with BD Accuri C6 Flow Cytometer (BD Biosciences).

Western blot analysis—Cells were lysed in either RIPA buffer (150 mM NaCl, 1.0% NP40 orTriton X-100,0.5% sodium deoxycholate, 0.1% SDS, 50 mM Tris, pH 8.0) or 1x Laemmli buffer (1% SDS, 10% glycerol, 100 mM TrisCl pH 7.5) supplemented with protease and phosphatase inhibitor cocktail (PPIC, a mixture of aprotinin at 1 μg/mL final concentration, leupeptin at 1 μg/mL final concentration, pepstatin at 1 μg/mL final concentration, trypsin inhibitor at 1 μg/mL final concentration, phenylmethylsulfonyl fluoride 50 μg/mL final concentration, sodium fluoride at 1 mM final concentration, and sodium orthovanadate at 0.1 mM final concentration). Crude lysates were briefly sonicated and spun down for 20 min at 18,000 g, followed by supernatant collection. 15 to 30 μg of protein was resolved on SDS-PAGE gels and transferred onto polyvinylidene difluoride membranes with a 0.45 μm pore size. Membranes were blocked with 3% BSA in Tris-buffered saline with 0.1% Tween 20 (TBS-T). Blots were probed with primary antibodies (see key resources table) overnight at 4°C diluted in blocking buffer. Antibodies detecting p53 and MDM4 were diluted in 3% BSA in 300 mM NaCl, 20 mM TrisCl pH 7.6, 0.1% Tween 20. Next, membranes were washed with TBS-T, incubated with HRP-conjugated secondary antibodies (see key resources table) diluted in blocking buffer, and washed again with TBS-T. The HRP signal was detected with the SuperSignal West Pico PLUS Chemiluminescent Substrate or Supersignal West Femto Maximum Sensitivity Chemiluminescent Substrate (ThermoFisher Scientific). The signal was captured using the ImageQuant LAS 4000LAS4000 digital imaging system (GE Healthcare).

Immunoprecipitation—Immunoprecipitation was performed in CHP212 WT stably transduced with the construct TetR and CMV/TO-3xFLAG-FAM193A constructs plated into 15 cm plates and allowed to reach ~90% confluency at time of collection (5 × 15 cm plates per sample). Prior to collection, 3xFLAG-FAM193A expression was induced with 2 μg/mL doxycyclinefor 48 h. Control or *FAM193A* KO CHP212 cells were plated into 15 cm plates and allowed to reach ~80% confluency and next, treated with either 0.05% DMSO (vehicle control) or 2.5 mM Nutlin-3afor 16h. Cells were washed twice with PBS and 1x with PBS with PPIC. Cells were scraped of and lysed in 150 mM NaCl, 1.0% NP40, and 50 mM Tris pH 8.0 with PPIC. Crude lysates were incubated on ice for 20 min, vortexed every few minutes and spun down for 20 min at 18,000 g at 4°C. After protein quantification with BCA, lysate protein concentration was equalized between samples and lysates precleared for 1 h at 4°C with: (a) mouse IgG agarose beads for FLAG immunoprecipitations or (b) Protein G Dynabeads for MDM4, MDM2, and p53 immunoprecipitations. Reaction set up: lysates were incubated overnight at 4°C with (a) anti-FLAG M2 Magnetic Beads or (b) anti-MDM4 IgG (or rabbit IgG control) with Protein G Dynabeads. Bead washes: (a) FLAG beads were washed 3x with TBS; (b) MDM4 IP beads were washed 4x with 150 mM NaCl, 1.0% NP40, and 50 mM Tris pH 8.0. Bound protein was released by incubating with Laemmli Sample Buffer diluted in TBS/wash buffer at 95°C for 5 min.

Halo-FAM193A pulldown—The cell lines selected for these experiments were selected based on their high transfection efficiency due to the fact that the open reading frame encoding Halo-FAM193A was too large for lentiviral vector packaging. HEK293FT or HCT116 cells were plated on 15 cm dishes at $7*10^6$-$1*10^7$ cells/dish. Following 24 h, cells were transfected with 15 μg of pDEST-CMV-Halo-FAM193A (or HaloFAM193A fragments) and/or pcDNA3.1-CMV-MDM4c3 (a gift from the Jiandong Chen laboratory) or pLX304-MDM4-V5 and incubated overnight as described in the Cell line generation section. Cells were collected at 48 h post-transfection (after 16 h of DMSO and/or 10 μM Nutlin treatment in HCT116 cells). Pulldowns were performed using the HaloTag Mammalian Pull-Down System according to manufacturer's instructions. Briefly, cells were collected, washed twice with PBS, and frozen at −80°C. Cell pellets were lysed in Mammalian Lysis + PIC (Promega) buffer, homogenized by passing through 23G needle and spun down at 15 min 18,000 g. If experiment included a Nutlin treatment step, lysates were quantified with BCA and diluted to ensure equal protein quantity. For proteolytic cleavage with PreScission protease, MDM4c3 lysates were incubated for 30 min with 20 units of protease at 4°C. Lysates were diluted with TBS and incubated with 80 μL HaloLink Resin for 25 min at room temperature (optional: 40 units of PreScission protease added to pulldown reaction). Resin was washed three times with TBS+0.5% NP40. Optional ProTeV digest step: resin was incubated with 30 units of ProTEV Plus Protease for 1 h at 25°C. Bound protein was released by incubating with SDS Elution Buffer (Promega) and Laemmli Sample Buffer at 95°C for 5 min. Identical experiments were done with MDM4 mutants lacking the last 8 amino acids (ΔC) or with the point mutation C463A. Mutants were generated from the MDM4c3 backbones using the primers listed in the key resources table. Presence of the deletion or point mutation was verified by Sanger sequencing.

Immunofluorescent detection of FAM193A—H4 WT and TetR TO/CMV-3xFLAG-FAM193A cells pre-treated with 2 μg/mL doxycycline for 48 h were plated onto 12 mm acid-etched coverslips in 24-well plates at $7*10^4$ cells/well with doxycycline in the cultivation media. After 48 h, cells were washed with ice-cold PBS with Ca^{2+} and Mg^{2+} and fixed for 15 min in 4% paraformaldehyde (PFA) in PBS on ice and then washed three times for 5 min with PBS. Next, coverslips were incubated for 10 min with 0.1 M ammonium chloride in PBS, washed twice in PBS for 3 min each time, permeabilized for 30 min with 0.5% Triton X-100 in PBS, washed again three times for 5 min in PBS, and once in TBS-T for additional 5 min. Samples were blocked for unspecific antibody binding for 1 h with 3% BSA in TBS-T and incubated overnight at 4°C with anti-FLAG diluted 1:250 in 3% BSA in TBS-T. Next, samples were washed five times for 5 min with TBS-T and incubated with goat-anti mouse IgG-Alexa Fluor 488 for 1 h in 3% BSA in TBS-T. After the incubation, coverslips were washed five times for 5 min with TBS-T, once for 5 min with PBS, incubated for 10 min in 4% PFA/PBS, and washed three times for 5 min in PBS. The last wash was followed by incubation with 0.1 M ammonium chloride in PBS for 10 min, two PBS washes (3 min each) and 5 min of nuclei staining with 1 μg/mL DAPI. Samples were washed with PBS and water just before affixing them to slides using Molecular Probes ProLong Gold Antifade Mountant. Finally, stained cells were imaged with Zeiss LSM780 confocal microscope system with a C-Apochromat 40x/1.20 W Korr FCS M27 objective.

Preparation of nuclear and cytoplasmic fractions—The following cell types were used for isolation of cellular fractions: HCT116 cells transfected with GFP/Halo-FAM193A, H4 cells transfected with TetR-TO-GFP/TO-3xFLAG-FAM193A, and CHP212 cells transfected with WT/TetR-TO-3xFLAG-FAM193A. Starting from 24 h after the transfections, cell cultures were maintained in media supplemented with 2 μg/mL doxycycline. Treated cells were detached by trypsinization and resuspended in ice-cold medium with 10% FBS. All following steps were performed on ice or at 4°C. Cell suspensions were spun down for 5 min at 300 g and resuspended in 10 mL of PBS. Next, cells were counted, diluted to ensure equal numbers across samples, and washed again with PBS. A fifth of the cell samples was saved for a total protein isolation with 1% NP40, 50 mM TrisCI pH 8.0,150 mM NaCI with PPIC. Total protein lysates were sonicated and centrifugated for 20 min at 18,000 g, 4°C. Remaining cells were incubated for 10 min in Buffer A (10 mM HEPES, 1.5 mM $MgCI_2$,10 mM KCI, 0.5% NP40, pH 7.9; with PPIC) and centrifuged at 1000 g for 10 min. Collected supernatant contained cytoplasmic fraction and pellets contained nuclei. Supernatants were centrifuged at 18,000 g for 20 min, supernatants were transferred to fresh tubes and assayed as cytoplasmic fractions. Pelleted nuclei from the first centrifugation step were washed twice with buffer A (each round for 10 min at 1000 g), resuspended in protein extraction Buffer B (5 mM HEPES, 1.5 mM $MgCl_2$, 0.2 mM EDTA, 26% glycerol (v/v), pH 7.9; with PPIC), and cleared of undissolved debris by centrifugation at 18,000 g for 20 min. Collected supernatants were assayed as nuclear fractions.

Cycloheximide chase assay—A549 or CHP212 (non-targeting control and *FAM193A* KO) cells were plated into 60 mm dishes at $1-1.5\times10^6$ cells/dish and following 48 h were treated with 25 μg/mL CHX. Cells were collected at 0, 1, 2, 4, 8, and 16 h of treatment by washing them with ice-cold PBS and lysing them with protein extraction buffer (1% NP40, 50 mM TrisCl pH 8.0,150 mM NaCl with PPIC). Samples were further processed as described in the “Western blot” section. Following Western blot analysis, levels of MDM4 and GAPDH were quantified using ImageJ (v 1.53a) using its Analyze-Gels tool.

Analysis of GTEx and TCGA gene expression data—Unified normalized gene expression level (FPKM) data of normal tissues and cancer samples (originally sourced from the Genotype Tissue Expression project (GTEx) and The Cancer Genome Atlas (TCGA)) was obtained from[57] (https://figshare.com/articles/dataset/Data_record_3/5330593). Descriptors of tissue or cancer types were included in the names of individual datafiles except for specific colon tissue types. To separate colon samples into sigmoid and transverse colon groups (control healthy tissues corresponding to rectum adenocarcinoma and colon adenocarcinoma, respectively), their IDs and descriptors were obtained from GTEx. Mean expressions between control and cancer samples were compared with two-sample Wilcoxon tests.

Analysis of *FAM193A* mutations and copy number variations—*FAM193A* and *TP53* alteration data was downloaded from CBioPortal by querying the Pan-Cancer Atlas Dataset. The data used to determine gene alterations included lists of mutations, copy-number alterations (CNA), structural variants, and altered and unaltered samples. Analysis

steps: (1) Determination of tumors with *FAM193A* alterations: alteration of *FAM193A* was determined based on CBioPortal "altered" vs. "unaltered" classification. These tumors included tumors that had either a mutation or structural alteration of *FAM193A* or a CNA equal to −2 or 2. (2) Selection of *TP53* WT tumors: tumors were considered WT if they were marked as "WT", the CNA was not equal −2, and didn't encode any structural variants. Tumors that were not assayed for CNA were excluded from the analysis. (3) Cancer type information was extracted from the "STUDY_ID" identifiers provided with the CBioPortal data or obtained the TCGA Pan-Cancer Clinical Data Resource (CBioPortal provided no distinction between COAD and READ tumor samples). Three tumor samples were assigned tumor types manually upon determining their types in the TCGA data portal (TCGA-5M-AAT5– 01 – COAD, TCGA-5M-AATA-01 – COAD; TCGA-F5-6810-01 – READ). (4) *FAM193A* Alterations were classified into 4 categories: (i) *FAM193A* mutated (ii) *FAM193A* CNA equal –2; (iii) *FAM193A* mutated and with CNA equal 2; (iv) *FAM193* WT and CNA equal 2. To generate the visualization of *FAM193A* mutation distribution along the FAM193A protein codding sequence mutation GDC Pan-Cancer (PANCAN) data was downloaded via Xena[102] platform due to its more comprehensive sequence annotations enabling full matching to the full length *FAM193A* ORF.

Cancer patient survival analysis—The cancer patient survival data source was the TCGA Pan-Cancer Clinical Data Resource.[59] *TP53* genetic alterations were determined based on mutation, CNA, and structural alteration data obtained from CBioPortal. Tumors were considered as WT if they were marked as "WT", with no CNAs, and didn't encode any structural variants. *FAM193A* mRNA expression data (z-scores relative to all samples) was obtained from CBioPortal. High vs. low *FAM193A* mRNA expression level splits were determined using the Log Rank statistic method with a distribution via a Monte-Carlo simulation. Survivals of *FAM193A* high- and low-expressing groups were compared with Log Rank statistics; p values were adjusted with the Benjamini-Hochberg procedure.

Cloning of *FAM193A* cDNA—The *FAM193A* cDNA was cloned by combining two fragments of the *FAM193A* cDNA because of a high GC content of the 5′ end the *FAM193A* ORF. The 3′ end of *FAM193A* (encoding from 220 bp onwards) was cloned from mRNA isolated from CHP212 with TRIzol reagent as follows: 5 μg of total RNA were treated with DNaseI and used in a reverse transcriptase reaction (SuperScript, IV, ThermoFisher Scientific) with primer FAM-211-ORF-R-UAG. Obtained cDNA has been used as a template in a gradient PCR reaction with primers FAM-211-ORF-F-ATG and FAM-211-ORF-R-UAG using Phusion High Fidelity DNA Polymerase (ThermoFisher Scientific). Next, the PCR product has been cloned into the pJET1.2 (ThermoFisher Scientific) vector and sequenced. The 5′ end of *FAM193A* cDNA was cloned from a gBlock (synthesized by Integrated DNA Technologies, Inc.) of the following sequence: 5′-TACCGAATTC GCGGCCGCAT GAGCCCAGCT GATGCGAAGC GCGGAGCGAA GCGAAGAAAG AATAAACGGG GGGGAGGAGG TGGCTCCGGG GGGGGTAACG GCGGAGCATC TTCTGGCAAA GCAGGACCCG CAGCTGCTTT GCGGGGCTCT CAGGCCGCAG GACTTGCAGC GCCCGGCAGC GCGGCTGGTC TTGTTGGGGG AGCTGCTGCG GCAAATGGGC CTTTGGGAGC AGGGGCAAGC GCAGGAGGTG CAGCTCCAGG CGGCTACTTC GAGACTCCTT TTAGTTTTGG CATGAATCAT

AGGACACCAC CCTACCCTGC TGGGGATTAT TGTCTTCTGT GCAGAAGTGA ACGGAAAGAC TCATCATTCT TAGAGAGTGG AATTAAGACT GCGAGCAAAT TGGCCCTTTC CATGGCTCCC AAGGGCAACA GCGTGCTGCA CCTGCCACTG TGGGTGTGCC CGGACTGCCG CAGGACCGTG GAGAAGGAGG AGAGGCATGG CGGCCTTGAC CAGCCAGTGA GCCAAGATTT TCTTCTTCAC TCCTCGCTTG GTGGCTCCCA GCCAGAGGCC GGCAGTGGTG GGAGGCTCGC TCTGGGTGCA CAGACGCTGC CTTCAGACAC CGCATGCTCG TGCGAGGCCT GCAGTGAGCG CAGAGAAATT TCGGCAGAGG CGGACCGGGA ACCTCAGCAG CTGCAGAACT ACTGGTCAGA AGTGCGCTAC ACGGTGCGCT GCATCTACCG CCAGGCAGGA ACCCCGCTGG CAGATGACCA GGACCAGTCT CTGGTGCCTG ACAAGGAGGG AGTGAAGGAG CTCGTGGATA GGCTC-3'. The gBlock contains NotI (5′ of FAM193A ATG) and SacI (occurring within the FAM193A ORF) restriction sites which were used to clone the 5′ end *FAM193A* cDNA into the pJET1.2 vector containing the 3′ end of *FAM193A.* The FAM193A cDNA was then cloned from pJet1.2 into pENTR4-FLAG (w210-2)[103] using restriction sites Notl and Xbal. The pENTR4-FLAG-FAM193A construct was next used as the base for 3xFLAG-FAM193, Halo-FAM193A and FAM193A fragment cloning.

3xFLAG-FAM193A construct generation—The 5′ 3xFLAG-tagged FAM193A generated through modification of pENTR4-Flag-FAM193A. The 5′ FLAG tag was removed by digesting the plasmid with Aflll and Notl restriction enzymes and cloning in a gBlock of the following sequence: 5'- CTACAAACTC TTCCTGTTAG TTAGTTACTT AAGCTCGGGC CCCAAATAAT GATTTTATTT TGACTGATAG TGACCTGTTC GTTGCAACAA ATTGA TAAGC AATGCTTTTT TATAATGCCA ACTTTGTACA AAAAAGCAGG CTCCACCATG CTCGGATCCA TGGGAACCAA TACCGG TTCA GTCGACTGGA TCCGGTACCG AATTCGCGGC CGCATGAGCC CAGCTGATGC GAAGCGCGGA -3′, creating the pENTR4-FAM193A plasmid. To create the pENTR4-5′ 3x-Flag-FAM193A, the pENTR4-FAM193A plasmid was digested using Agel and Notl, and a gBlock: '5- CCACCATGCT CGGATCCATG GGAACCAATA CCGGTGTTTC AGGAAGCGGA GATTACAAGG ATGACGACGA TAAGGGCGAT TACAAGGATG ACGACGATAA GGGAGATTAC AAGGATGACG ACGATAAGTC AGGCTCAGGC ATGAGCCCAG CTGATGC -3′, was Gibson assembled into the cut site. The 5′ 3x-Flag-FAM193A was shuttled into pLenti-CMV/TO-Puro-DEST (670-1) (Addgene #17293)[103] using Gateway LR cloning to create the pLenti-CMV/TO-3xFLAG-FAM193A-Puro.

Halo-FAM193A construct generation—FAM193A was cloned intopENTR4-HaloTag (w876-1) (Addgene #29644). First, FAM193A insert was produced by PCR using primers FAM-Notl-noATG-FWD and FAM-Xbal-REV with Phusion High Fidelity DNA Polymerase (ThermoFisher Scientific). PCR product was cloned into pENTR4-HaloTag by restriction cloning into Notl and Xbal sites. Resultant Halo-FAM193A ORF was transferred into pDEST-CMV-polysite (Addgene #122843) via recombination catalyzed by Gateway LR Clonase ll Plus enzyme (ThermoFisher Scientific).

Cloning of FAM193A fragments—Fragments of the FAM193A ORF were subcloned by PCR amplification using Phusion High Fidelity DNA Polymerase with the following primer

pairs: fragment 1: FAM1-BamHl-FWD and FAM1-Xbal-REV; fragment 2: FAM2-EcoRl-FWD and FAM2-Xbal-REV; fragment 3: FAM3-BamHl-FWD and FAM3-Xbal-REV; fragment 4: FAM4-BamHl-FWD and FAM4-Xbal-REV; fragment 5: FAM5-BamHl-FWD and FAM5-Xbal-REV. Resultant PCR fragments were subcloned into pENTR4-HaloTag (w876–1; Addgene) into BamHl/Xbal (fragment 1,3,4, and 5) or EcoRl/Xbal (fragment 2) sites. Resultant Halo-FAM193A fragment ORFs was transferred into pDEST-CMV-polysite (Addgene #122843) via recombination catalyzed by Gateway LR Clonase ll Plus enzyme (ThermoFisher Scientific).

QUANTIFICATION AND STATISTICAL ANALYSIS

All analysis has been performed in R Studio. Statistical details (n, representation of n, and statistic tests, correction methods, and definitions of center and dispersion) were included in the METHODS DETAILS section in each subsection where applicable and in the figure legends.

Results were considered significant with p values <0.05 with the following annotations *p < 0.05, **p < 0.01, and ***p < 0.001.

Supplementary Material

Refer to Web version on PubMed Central for supplementary material.

ACKNOWLEDGMENTS

This work was supported primarily by NIH grant R01CA117907 to the Wings of Hope for Pancreatic Research Foundation, the Cancer League of Colorado, the Global Down Syndrome Foundation, and the Anna and John J. Sie Foundation. This work was supported by the Functional Genomics Shared Resource, the Flow Cytometry Shared Resource, and the Genomics Shared Resource of the University of Colorado Cancer Center through grant P30CA046934. Imaging was performed in the Advanced Light Microscopy Core Facility of the University of Colorado Neuro Technology Center supported in part by grants P30 NS048154 and P30 DK116073. We thank Dr. Jiandong Chen for the generous gift of the MDM4c3 plasmid used in this study. The graphical abstract was created with BioRender.

INCLUSION AND DIVERSITY

We support inclusive, diverse, and equitable conduct of research.

REFERENCES

1. Cerami E, Gao J, Dogrusoz U, Gross BE, Sumer SO, Aksoy BA, Jacobsen A, Byrne CJ, Heuer ML, Larsson E, et al. (2012). The cBio cancer genomics portal: an open platform for exploring multidimensional cancer genomics data. Cancer Discov. 2, 401–404. 10.1158/2159-8290.CD-12-0095. [PubMed: 22588877]
2. Gao J, Aksoy BA, Dogrusoz U, Dresdner G, Gross B, Sumer SO, Sun Y, Jacobsen A, Sinha R, Larsson E, et al. (2013). Integrative analysis of complex cancer genomics and clinical profiles using the cBioPortal. Sci. Signal. 6, pl1. 10.1126/scisignal.2004088. [PubMed: 23550210]
3. Hainaut P, and Pfeifer GP (2016). SomaticTP53 mutations in the era of genome sequencing. Cold Spring Harb. Perspect. Med. 6, a026179. 10.1101/cshperspect.a026179. [PubMed: 27503997]
4. Vogelstein B, Lane D, and Levine AJ (2000). Surfing the p53 network. Nature 408, 307–310. 10.1038/35042675. [PubMed: 11099028]

5. Sullivan KD, Galbraith MD, Andrysik Z, and Espinosa JM (2018). Mechanisms of transcriptional regulation by p53. Cell Death Differ. 25, 133–143. 10.1038/cdd.2017.174. [PubMed: 29125602]
6. Andrysik Z, Galbraith MD, Guarnieri AL, Zaccara S, Sullivan KD, Pandey A, MacBeth M, Inga A, and Espinosa JM (2017). Identification of a core TP53 transcriptional program with highly distributed tumor suppressive activity. Genome Res. 27, 1645–1657. 10.1101/gr.220533.117. [PubMed: 28904012]
7. Oliner JD, Pietenpol JA, Thiagalingam S, Gyuris J, Kinzler KW, and Vogelstein B (1993). Oncoprotein MDM2 conceals the activation domain of tumour suppressor p53. Nature 362, 857–860. 10.1038/362857a0. [PubMed: 8479525]
8. Kubbutat MH, Jones SN, and Vousden KH (1997). Regulation of p53 stability by Mdm2. Nature 387, 299–303. 10.1038/387299a0. [PubMed: 9153396]
9. Ohtsubo C, Shiokawa D, Kodama M, Gaiddon C, Nakagama H, Jochemsen AG, Taya Y, and Okamoto K (2009). Cytoplasmic tethering is involved in synergistic inhibition of p53 by Mdmx and Mdm2. Cancer Sci. 100, 1291–1299. 10.1111/j.1349-7006.2009.01180.x. [PubMed: 19432880]
10. Iyappan S, Wollscheid HP, Rojas-Fernandez A, Marquardt A, Tang HC, Singh RK, and Scheffner M (2010). Turning the RING domain protein MdmX into an active ubiquitin-protein ligase. J. Biol. Chem. 285, 33065–33072. 10.1074/jbc.M110.115113. [PubMed: 20705607]
11. Zauberman A, Flusberg D, Haupt Y, Barak Y, and Oren M (1995). A functional p53-responsive intronic promoter is contained within the human mdm2 gene. Nucleic Acids Res. 23, 2584–2592. 10.1093/nar/23.14.2584. [PubMed: 7651818]
12. Montes de Oca Luna R, Wagner DS, and Lozano G (1995). Rescue of early embryonic lethality in mdm2-deficient mice by deletion of p53. Nature 378, 203–206. 10.1038/378203a0. [PubMed: 7477326]
13. Jones SN, Roe AE, Donehower LA, and Bradley A (1995). Rescue of embryonic lethality in Mdm2-deficient mice by absence of p53. Nature 378, 206–208. 10.1038/378206a0. [PubMed: 7477327]
14. Parant J, Chavez-Reyes A, Little NA, Yan W, Reinke V, Jochemsen AG, and Lozano G (2001). Rescue of embryonic lethality in Mdm4-null mice by loss of Trp53 suggests a nonoverlapping pathway with MDM2 to regulate p53. Nat. Genet. 29, 92–95. 10.1038/ng714. [PubMed: 11528400]
15. Finch RA, Donoviel DB, Potter D, Shi M, Fan A, Freed DD, Wang CY, Zambrowicz BP, Ramirez-Solis R, Sands AT, and Zhang N (2002). mdmx is a negative regulator of p53 activity in vivo. Cancer Res. 62, 3221–3225. [PubMed: 12036937]
16. Migliorini D, Lazzerini Denchi E, Danovi D, Jochemsen A, Capillo M, Gobbi A, Helin K, Pelicci PG, and Marine JC (2002). Mdm4 (Mdmx) regulates p53-induced growth arrest and neuronal cell death during early embryonic mouse development. Mol. Cell Biol. 22, 5527–5538. 10.1128/MCB.22.15.5527-5538.2002. [PubMed: 12101245]
17. Grier JD, Xiong S, Elizondo-Fraire AC, Parant JM, and Lozano G (2006). Tissue-specific differences of p53 inhibition by Mdm2 and Mdm4. Mol. Cell Biol. 26, 192–198. 10.1128/MCB.26.1.192-198.2006. [PubMed: 16354690]
18. Boesten LSM, Zadelaar SM, De Clercq S, Francoz S, van Nieuwkoop A, Biessen EAL, Hofmann F, Feil S, Feil R, Jochemsen AG, et al. (2006). Mdm2, but not Mdm4, protects terminally differentiated smooth muscle cells from p53-mediated caspase-3-independent cell death. Cell Death Differ. 13, 2089–2098. 10.1038/sj.cdd.4401973. [PubMed: 16729027]
19. Xiong S, Van Pelt CS, Elizondo-Fraire AC, Fernandez-Garcia B, and Lozano G (2007). Loss of Mdm4 results in p53-dependent dilated cardiomyopathy. Circulation 115, 2925–2930. 10.1161/CIRCULATIONAHA.107.689901. [PubMed: 17533180]
20. Barboza JA, Iwakuma T, Terzian T, El-Naggar AK, and Lozano G (2008). Mdm2 and Mdm4 loss regulates distinct p53 activities. Mol. Cancer Res. 6, 947–954. 10.1158/1541-7786.MCR-07-2079. [PubMed: 18567799]
21. Vassilev LT, Vu BT, Graves B, Carvajal D, Podlaski F, Filipovic Z, Kong N, Kammlott U, Lukacs C, Klein C, et al. (2004). In vivo activation of the p53 pathway by small-molecule antagonists of MDM2. Science 303, 844–848. 10.1126/science.1092472. [PubMed: 14704432]

22. Sanz G, Singh M, Peuget S, and Selivanova G (2019). Inhibition of p53 inhibitors: progress, challenges and perspectives. J. Mol. Cell Biol. 77, 586–599. 10.1093/jmcb/mjz075

23. Tovar C, Rosinski J, Filipovic Z, Higgins B, Kolinsky K, Hilton H, Zhao X, Vu BT, Qing W, Packman K, et al. (2006). Small-molecule MDM2 antagonists reveal aberrant p53 signaling in cancer: implications for therapy. Proc. Natl. Acad. Sci. USA 103, 1888–1893. 10.1073/pnas.0507493103. [PubMed: 16443686]

24. Skalniak L, Kocik J, Polak J, Skalniak A, Rak M, Wolnicka-Glubisz A, and Holak TA (2018). Prolonged idasanutlin (RG7388) treatment leads to the generation of p53-mutated cells. Cancers 10, 396. 10.3390/cancers10110396. [PubMed: 30352966]

25. Kucab JE, Hollstein M, Arlt VM, and Phillips DH (2017). Nutlin-3a selects for cells harbouring TP53 mutations. Int. J. Cancer 140, 877–887. 10.1002/ijc.30504. [PubMed: 27813088]

26. Laroche A, Tran-Cong K, Chaire V, Lagarde P, Hostein I, Coindre JM, Chibon F, Neuville A, Lesluyes T, Lucchesi C, and Italiano A (2015). Heterogeneous mechanisms of secondary resistance and clonal selection in sarcoma during treatment with nutlin. PLoS One 10, e0137794. 10.1371/journal.pone.0137794. [PubMed: 26427052]

27. Jung J, Lee JS, Dickson MA, Schwartz GK, Le Cesne A, Varga A, Bahleda R, Wagner AJ, Choy E, de Jonge MJ, et al. (2016). TP53 mutations emerge with HDM2 inhibitor SAR405838 treatment in de-differentiated liposarcoma. Nat. Commun. 7, 12609. 10.1038/ncomms12609. [PubMed: 27576846]

28. Allen MA, Andrysik Z, Dengler VL, Mellert HS, Guarnieri A, Freeman JA, Sullivan KD, Galbraith MD, Luo X, Kraus WL, et al. (2014). Global analysis of p53-regulated transcription identifies its direct targets and unexpected regulatory mechanisms. Elife 3, e02200. 10.7554/eLife.02200. [PubMed: 24867637]

29. Du W, Wu J, Walsh EM, Zhang Y, Chen CY, and Xiao ZXJ (2009). Nutlin-3 affects expression and function of retinoblastoma protein: role of retinoblastoma protein in cellular response to nutlin-3. J. Biol. Chem. 284, 26315–26321, M109.046904 [pii]. 10.1074/jbc.M109.046904. [PubMed: 19648117]

30. París R, Henry RE, Stephens SJ, McBryde M, and Espinosa JM (2008). Multiple p53-independent gene silencing mechanisms define the cellular response to p53 activation. Cell Cycle 7, 2427–2433. 10.4161/cc.6420. [PubMed: 18677110]

31. Henry RE, Andrysik Z, París R, Galbraith MD, and Espinosa JM (2012). A DR4:tBID axis drives the p53 apoptotic response by promoting oligomerization of poised BAX. EMBO J. 31,1266–1278. 10.1038/emboj.2011.498. [PubMed: 22246181]

32. Wade M, Rodewald LW, Espinosa JM, and Wahl GM (2008). BH3 activation blocks Hdmx suppression of apoptosis and cooperates with Nutlin to induce cell death. Cell Cycle 7, 1973–1982. [PubMed: 18604177]

33. Andrysik Z, Kim J, Tan AC, and Espinosa JM (2013). A genetic screen identifies TCF3/E2A and TRIAP1 as pathway-specific regulators of the cellular response to p53 activation. Cell Rep. 3, 1346–1354. 10.1016/j.celrep.2013.04.014. [PubMed: 23684607]

34. Sullivan KD, Palaniappan VV, and Espinosa JM (2015). ATM regulates cell fate choice upon p53 activation by modulating mitochondrial turnover and ROS levels. Cell Cycle 14, 56–63. 10.4161/15384101.2014.973330. [PubMed: 25483068]

35. Nakano K, and Vousden KH (2001). PUMA, a novel proapoptotic gene, is induced by p53. Mol. Cell 7, 683–694. 10.1016/s1097-2765(01)00214-3. [PubMed: 11463392]

36. Yu J, Zhang L, Hwang PM, Kinzler KW, and Vogelstein B (2001). PUMA induces the rapid apoptosis of colorectal cancer cells. Mol. Cell 7, 673–682. 10.1016/s1097-2765(01)00213-1. [PubMed: 11463391]

37. Yang W, Soares J, Greninger P, Edelman EJ, Lightfoot H, Forbes S, Bindal N, Beare D, Smith JA, Thompson IR, et al. (2013). Genomics of Drug Sensitivity in Cancer (GDSC): a resource for therapeutic biomarker discovery in cancer cells. Nucleic Acids Res. 41, D955–D961. 10.1093/nar/gks1111. [PubMed: 23180760]

38. Ray-Coquard I, Blay JY, Italiano A, Le Cesne A, Penel N, Zhi J, Heil F, Rueger R, Graves B, Ding M, et al. (2012). Effect of the MDM2 antagonist RG7112 on the P53 pathway in patients with MDM2-amplified, well-differentiated or dedifferentiated liposarcoma: an exploratory proof-

of-mechanism study. Lancet Oncol. 13, 1133–1140. 10.1016/S1470-2045(12)70474-6. [PubMed: 23084521]

39. Pishas KI, Neuhaus SJ, Clayer MT, Schreiber AW, Lawrence DM, Perugini M, Whitfield RJ, Farshid G, Manavis J, Chryssidis, 5., et al. (2014). Nutlin-3a efficacy in sarcoma predicted by transcriptomic and epigenetic profiling. Cancer Res. 74, 921–931. 10.1158/0008-5472.CAN-13-2424. [PubMed: 24336067]
40. Ishizawa J, Nakamaru K, Seki T, Tazaki K, Kojima K, Chachad D, Zhao R, Heese L, Ma W, Ma MCJ, et al. (2018). Predictive gene signatures determine tumor sensitivity to MDM2 inhibition. Cancer Res. 78, 2721–2731. 10.1158/0008-5472.CAN-17-0949. [PubMed: 29490944]
41. Jeay S, Gaulis S, Ferretti S, Bitter H, Ito M, Valat T, Murakami M, Ruetz S, Guthy DA, Rynn C, et al. (2015). A distinct p53 target gene set predicts for response to the selective p53-HDM2 inhibitor NVP-CGM097. Elife 4, e06498. 10.7554/eLife.06498. [PubMed: 25965177]
42. Wade M, Li YC, and Wahl GM (2013). MDM2, MDMX and p53 in oncogenesis and cancer therapy. Nat. Rev. Cancer 13, 83–96. 10.1038/nrc3430. [PubMed: 23303139]
43. Shalem O, Sanjana NE, Hartenian E, Shi X, Scott DA, Mikkelson T, Heckl D, Ebert BL, Root DE, Doench JG, and Zhang F (2014). Genome-scale CRISPR-Cas9 knockout screening in human cells. Science 343, 84–87. 10.1126/science.1247005. [PubMed: 24336571]
44. Janic A, Valente LJ, Wakefield MJ, Di Stefano L, Milla L, Wilcox 5, Yang H, Tai L, Vandenberg CJ, Kueh AJ, et al. (2018). DNA repair processes are critical mediators of p53-dependent tumor suppression. Nat. Med. 24, 947–953. 10.1038/s41591-018-0043-5. [PubMed: 29892060]
45. Dempster JM, Rossen J, Kazachkova M, Pan J, Kugener G, Root DE, and Tsherniak A (2019). Extracting biological insights from the project achilles genome-scale CRISPR screens in cancer cell lines. Preprint at bioRxiv. 10.1101/720243.
46. Wade M, Wong ET, Tang M, Stommel JM, and Wahl GM (2006). Hdmx modulates the outcome of p53 activation in human tumor cells. J. Biol. Chem. 281, 33036–33044. 10.1074/jbc.M605405200. [PubMed: 16905769]
47. Stark C, Breitkreutz BJ, Reguly T, Boucher L, Breitkreutz A, and Tyers M (2006). BioGRID: a general repository for interaction datasets. Nucleic Acids Res. 34, D535–D539. 10.1093/nar/gkj109. [PubMed: 16381927]
48. Orchard S, Ammari M, Aranda B, Breuza L, Briganti L, Broackes-Carter F, Campbell NH, Chavali G, Chen C, del-Toro N, et al. (2014). The MIntAct project-IntAct as a common curation platform for 11 molecular interaction databases. Nucleic Acids Res. 42, D358–D363. 10.1093/nar/gkt1115. [PubMed: 24234451]
49. Huttlin EL, Bruckner RJ, Paulo JA, Cannon JR, Ting L, Baltier K, Colby G, Gebreab F, Gygi MP, Parzen H, et al. (2017). Architecture of the human interactome defines protein communities and disease networks. Nature 545, 505–509. 10.1038/nature22366. [PubMed: 28514442]
50. Huttlin EL, Bruckner RJ, Navarrete-Perea J, Cannon JR, Baltier K, Gebreab F, Gygi MP, Thornock A, Zarraga G, Tam S, et al. (2021). Dual proteome-scale networks reveal cell-specific remodeling of the human interactome. Cell 184, 3022–3040.e28. 10.1016/j.cell.2021.04.011. [PubMed: 33961781]
51. Piovesan D, Necci M, Escobedo N, Monzon AM, Hatos A, Mičetić 1, Quaglia F, Paladin L, Ramasamy P, Dosztányi Z, et al. (2021). MobiDB: intrinsically disordered proteins in 2021. Nucleic Acids Res. 49, D361–D367. 10.1093/nar/gkaa1058. [PubMed: 33237329]
52. Wei X, Wu S, Song T, Chen L, Gao M, Borcherds W, Daughdrill GW, and Chen J (2016). Secondary interaction between MDMX and p53 core domain inhibits p53 DNA binding. Proc. Natl. Acad. Sci. USA 113, E2558–E2563. 10.1073/pnas.1603838113. [PubMed: 27114532]
53. Liu X, Huang Q, Chen L, Zhang H, Schonbrunn E, and Chen J (2020). Tumor-derived CKIalpha mutations enhance MDMX inhibition of p53. Oncogene 39, 176–186. 10.1038/s41388-019-0979-z. [PubMed: 31462704]
54. Huang L, Yan Z, Liao X, Li Y, Yang J, Wang ZG, Zuo Y, Kawai H, Shadfan M, Ganapathy S, and Yuan ZM (2011).The p53 inhibitors MDM2/MDMX complex is required for control of p53 activity in vivo. Proc. Natl. Acad. Sci. USA 708, 12001–12006. 10.1073/pnas.1102309108.

55. Kawai H, Lopez-Pajares V, Kim MM, Wiederschain D, and Yuan ZM (2007). RING domain-mediated interaction is a requirement for MDM2's E3 ligase activity. Cancer Res. 67, 6026–6030. 10.1158/0008-5472.CAN-07-1313. [PubMed: 17616658]
56. Linke K, Mace PD, Smith CA, Vaux DL, Silke J, and Day CL (2008). Structure of the MDM2/MDMX RING domain heterodimer reveals dimerization is required for their ubiquitylation in trans. Cell Death Differ. 75, 841–848. 10.1038/sj.cdd.4402309.
57. Wang Q, Armenia J, Zhang C, Penson AV, Reznik E, Zhang L, Minet T, Ochoa A, Gross BE, lacobuzio-Donahue CA, et al. (2018). Unifying cancer and normal RNA sequencing data from different sources. Sci. Data 5, 180061. 10.1038/sdata.2018.61. [PubMed: 29664468]
58. Cancer Genome Atlas Research Network; Weinstein JN, Collisson EA, Mills GB, Shaw KRM, Ozenberger BA, Ellrott K, Shmulevich I, Sander C, and Stuart JM (2013). The cancer genome Atlas pan-cancer analysis project. Nat. Genet. 45, 1113–1120. 10.1038/ng.2764. [PubMed: 24071849]
59. Liu J, Lichtenberg T, Hoadley KA, Poisson LM, Lazar AJ, Cherniack AD, Kovatich AJ, Benz CC, Levine DA, Lee AV, et al. (2018). An integrated TCGA pan-cancer clinical data resource to drive high-quality survival outcome analytics. Cell 173, 400–416.e11. 10.1016/j.cell.2018.02.052. [PubMed: 29625055]
60. Welander J, Söderkvist P, and Gimm O (2011). Genetics and clinical characteristics of hereditary pheochromocytomas and paragangliomas. Endocr. Relat. Cancer 18, R253–R276. 10.1530/ERC-11-0170. [PubMed: 22041710]
61. Lane DP, and Crawford LV (1979). T antigen is bound to a host protein in SV40-transformed cells. Nature 278, 261–263. 10.1038/278261a0. [PubMed: 218111]
62. Kress M, May E, Cassingena R, and May P (1979). Simian virus 40-transformed cells express new species of proteins precipitable by anti-simian virus 40 tumor serum. J. Virol. 37, 472–483. 10.1128/jvi.31.2.472-483.1979.
63. Linzer DI, and Levine AJ (1979). Characterization of a 54K dalton cellular SV40 tumor antigen present in SV40-transformed cells and uninfected embryonal carcinoma cells. Cell 17, 43–52. 10.1016/0092-8674(79)90293-9. [PubMed: 222475]
64. Tchelebi L, Ashamalla H, and Graves PR (2014). Mutant p53 and the response to chemotherapy and radiation. Subcell. Biochem. 85, 133–159. 10.1007/978-94-017-9211-0_8. [PubMed: 25201193]
65. Zhong H, Chen G, Jukofsky L, Geho D, Han SW, Birzele F, Bader S, Himmelein L, Cai J, Albertyn Z, et al. (2015). MDM2 antagonist clinical response association with a gene expression signature in acute myeloid leukaemia. Br. J. Haematol. 171, 432–435. 10.1111/bjh.13411. [PubMed: 25855517]
66. Fogeron ML, Müller H, Schade S, Dreher F, Lehmann V, Kühnel A, Scholz AK, Kashofer K, Zerck A, Fauler B, et al. (2013). LGALS3BP regulates centriole biogenesis and centrosome hypertrophy in cancer cells. Nat. Commun. 4, 1531. 10.1038/ncomms2517. [PubMed: 23443559]
67. Liu J, Guan D, Dong M, Yang J, Wei H, Liang Q, Song L, Xu L, Bai J, Liu C, et al. (2020). UFMylation maintains tumour suppressor p53 stability by antagonizing its ubiquitination. Nat. Cell Biol. 22, 1056–1063. 10.1038/s41556-020-0559-z. [PubMed: 32807901]
68. Rodriguez J, Pilkington R, Garcia Munoz A, Nguyen LK, Rauch N, Kennedy S, Monsefi N, Herrero A, Taylor CT, and von Kriegsheim A (2016). Substrate-trapped interactors of PHD3 and FIH cluster in distinct signaling pathways. Cell Rep. 14, 2745–2760. 10.1016/j.celrep.2016.02.043. [PubMed: 26972000]
69. Chapman RM, Tinsley CL, Hill MJ, Forrest MP, Tansey KE, Pardiñas AF, Rees E, Doyle AM, Wilkinson LS, Owen MJ, et al. (2019). Convergent evidence that ZNF804A is a regulator of pre-messenger RNA processing and gene expression. Schizophr. Bull. 45, 1267–1278. 10.1093/schbul/sby183. [PubMed: 30597088]
70. Westberg C, Yang JP, Tang H, Reddy TR, and Wong-Staal F (2000). A novel shuttle protein binds to RNA helicase A and activates the retroviral constitutive transport element. J. Biol. Chem. 275, 21396–21401. 10.1074/jbc.M909887199. [PubMed: 10748171]

71. Han I, Xue Y, Harada S, Orstavik S, Skalhegg B, and Kieff E (2002). Protein kinase A associates with HA95 and affects transcriptional coactivation by Epstein-Barr virus nuclear proteins. Mol. Cell Biol. 22, 2136–2146. 10.1128/MCB.22.7.2136-2146.2002. [PubMed: 11884601]
72. Martins S, Eikvar S, Furukawa K, and Collas P (2003). HA95 and LAP2 beta mediate a novel chromatin-nuclear envelope interaction implicated in initiation of DNA replication. J. Cell Biol. 760, 177–188. 10.1083/jcb.200210026.
73. Melick CH, Meng D, and Jewell JL (2020). A-kinase anchoring protein 8L interacts with mTORC1 and promotes cell growth. J. Biol. Chem. 295, 8096–8105. 10.1074/jbc.AC120.012595. [PubMed: 32312749]
74. Kaplan N, Dong Y, Wang S, Yang W, Park JK, Wang J, Fiolek E, Perez White B, Chandel NS, Peng H, and Lavker RM (2020). FIH-1 engages novel binding partners to positively influence epithelial proliferation via p63. Faseb. J. 34, 525–539. 10.1096/fj.201901512R. [PubMed: 31914679]
75. Janke K, Brockmeier U, Kuhlmann K, Eisenacher M, Nolde J, Meyer HE, Mairbäurl H, and Metzen E (2013). Factor inhibiting HIF-1 (FIH-1) modulates protein interactions of apoptosis-stimulating p53 binding protein 2 (ASPP2). J. Cell Sci. 126, 2629–2640. 10.1242/jcs.117564. [PubMed: 23606740]
76. Hannes F, Hammond P, Quarrell O, Fryns JP, Devriendt K, and Vermeesch JR (2012). A microdeletion proximal of the critical deletion region is associated with mild Wolf-Hirschhorn syndrome. Am. J. Med. Genet. 158A, 996–1004. 10.1002/ajmg.a.35299. [PubMed: 22438245]
77. Reis V.N. d.S.,Kitajima JP, Tahira AC, Feio-Dos-Santos AC, Fock RA, Lisboa BCG, Simões SN, Krepischi ACV, Rosenberg C, Lourenco NC, et al. (2017). Integrative variation analysis reveals that a complex genotype may specify phenotype in siblings with syndromic autism spectrum disorder. PLoS One 12, e0170386. 10.1371/journal.pone.0170386. [PubMed: 28118382]
78. Lee KH, Kim SH, Kim CH, Min BJ, Kim GJ, Lim Y, Kim HS, Ahn KM, and Kim JH (2019). Identifying genetic variants underlying medication-induced osteonecrosis of the jaw in cancer and osteoporosis: a case control study. J. Transl. Med. 17, 381. 10.1186/s12967-019-2129-3. [PubMed: 31747953]
79. Guevara EE, Hopkins WD, Hof PR, Ely JJ, Bradley BJ, and Sherwood CC (2021). Comparative analysis reveals distinctive epigenetic features of the human cerebellum. PLoS Genet. 17, e1009506. 10.1371/journal.pgen.1009506. [PubMed: 33956822]
80. Amin M, Uhlig HH, Kamprad M, Karbe J, Osman AA, Grahmann F, Hummelsheim H, and Mothes T (2001). Neurological disease-associated autoantibodies against an unknown protein encoded by a RES4–22 homologous gene. Scand. J. Immunol. 53, 204–208. 10.1046/j.1365-3083.2001.00839.x. [PubMed: 11169226]
81. Youn JY, Dunham WH, Hong SJ, Knight JDR, Bashkurov M, Chen GI, Bagci H, Rathod B, MacLeod G, Eng SWM, et al. (2018). High-density proximity mapping reveals the subcellular organization of mRNA-associated granules and bodies. Mol. Cell 69, 517–532.e11. 10.1016/j.molcel.2017.12.020. [PubMed: 29395067]
82. Collart MA (2016). The Ccr4-Not complex is a key regulator of eukaryotic gene expression. Wiley Interdiscip Rev RNA 7, 438–454. 10.1002/wrna.1332. [PubMed: 26821858]
83. Shirai YT, Suzuki T, Morita M, Takahashi A, and Yamamoto T (2014). Multifunctional roles of the mammalian CCR4-NOT complex in physiological phenomena. Front. Genet. 5, 286. 10.3389/fgene.2014.00286. [PubMed: 25191340]
84. Zaccara S, Tebaldi T, Pederiva C, Ciribilli Y, Bisio A, and Inga A (2014). p53-directed translational control can shape and expand the universe of p53 target genes. Cell Death Differ. 21, 1522–1534. 10.1038/cdd.2014.79. [PubMed: 24926617]
85. Afroz T, Skrisovska L, Belloc E, Guillén-Boixet J, Méndez R, and Allain FHT (2014). A fly trap mechanism provides sequence-specific RNA recognition by CPEB proteins. Genes Dev. 28, 1498–1514. 10.1101/gad.241133.114. [PubMed: 24990967]
86. Novoa I, Gallego J, Ferreira PG, and Mendez R (2010). Mitotic cell-cycle progression is regulated by CPEB1 and CPEB4-dependent translational control. Nat. Cell Biol. 12, 447–56. 10.1038/ncb2046. [PubMed: 20364142]

87. Kim KM, Cho H, Choi K, Kim J, Kim BW, Ko YG, Jang SK, and Kim YK (2009). A new MIF4G domain-containing protein, CTIF, directs nuclear cap-binding protein CBP80/20-dependent translation. Genes Dev. 23, 2033–2045. 10.1101/gad.1823409. [PubMed: 19648179]

88. Sharp DA, Kratowicz SA, Sank MJ, and George DL (1999). Stabilization of the MDM2 oncoprotein by interaction with the structurally related MDMX protein. J. Biol. Chem. 274, 38189–38196. 10.1074/jbc.274.53.38189. [PubMed: 10608892]

89. Linares LK, Hengstermann A, Ciechanover A, Müller S, and Scheffner M (2003). HdmX stimulates Hdm2-mediated ubiquitination and degradation of p53. Proc. Natl. Acad. Sci. USA 100, 12009–12014. 10.1073/pnas.2030930100. [PubMed: 14507994]

90. Pant V, Xiong S, Iwakuma T, Quintás-Cardama A, and Lozano G (2011). Heterodimerization of Mdm2 and Mdm4 is critical for regulating p53 activity during embryogenesis but dispensable for p53 and Mdm2 stability. Proc. Natl. Acad. Sci. USA 108, 11995–12000. 10.1073/pnas.1102241108. [PubMed: 21730132]

91. Cancer Genome Atlas Research Network (2012). Comprehensive genomic characterization of squamous cell lung cancers. Nature 489, 519–525. 10.1038/nature11404. [PubMed: 22960745]

92. Cancer Genome Atlas Research Network (2014). Comprehensive molecular characterization of urothelial bladder carcinoma. Nature 507, 315–322. 10.1038/nature12965. [PubMed: 24476821]

93. Fujimoto K, Yamada Y, Okajima E, Kakizoe T, Sasaki H, Sugimura T, and Terada M (1992). Frequent association of p53 gene mutation in invasive bladder cancer. Cancer Res. 52, 1393–1398. [PubMed: 1540947]

94. Wu G, Wang F, Li K, Li S, Zhao C, Fan C, and Wang J (2019). Significance of TP53 mutation in bladder cancer disease progression and drug selection. PeerJ 7, e8261. 10.7717/peerj.8261. [PubMed: 31871844]

95. Cancer Genome Atlas Research Network; Kandoth C, Schultz N, Cherniack AD, Akbani R, Liu Y, Shen H, Robertson AG, Pashtan I, Shen., et al. (2013). Integrated genomic characterization of endometrial carcinoma. Nature 497, 67–73. 10.1038/nature12113. [PubMed: 23636398]

96. Iorio F, Knijnenburg TA, Vis DJ, Bignell GR, Menden MP, Schubert M, Aben N, Goncalves E, Barthorpe S, Lightfoot H, et al. (2016). A landscape of pharmacogenomic interactions in cancer. Cell 766, 740–754. 10.1016/j.cell.2016.06.017.

97. Barretina J, Caponigro G, Stransky N,Venkatesan K, Margolin AA, Kim S, Wilson CJ, Lehar J, Kryukov GV, Sonkin D, et al. (2012). The Cancer Cell Line Encyclopedia enables predictive modelling of anticancer drug sensitivity. Nature 483, 603–607. 10.1038/nature11003. [PubMed: 22460905]

98. Subramanian A, Tamayo P, Mootha VK, Mukherjee S, Ebert BL, Gillette MA, Paulovich A, Pomeroy SL, Golub TR, Lander ES, and Mesirov JP (2005). Gene set enrichment analysis: a knowledge-based approach for interpreting genome-wide expression profiles. Proc. Natl. Acad. Sci. USA 702, 15545–15550. 10.1073/pnas.0506580102.

99. Sanjana NE, Shalem O, and Zhang F (2014). Improved vectors and genome-wide libraries for CRISPR screening. Nat. Methods 11, 783–784. 10.1038/nmeth.3047. [PubMed: 25075903]

100. Abraham CG, Ludwig MP, Andrysik Z, Pandey A, Joshi M, Galbraith MD, Sullivan KD, and Espinosa JM (2018). DeltaNp63alpha suppresses TGFB2 expression and RHOA activity to drive cell proliferation in squamous cell carcinomas. Cell Rep. 24, 3224–3236. 10.1016/j.celrep.2018.08.058. [PubMed: 30232004]

101. Ran FA, Hsu PD, Wright J, Agarwala V, Scott DA, and Zhang F (2013). Genome engineering using the CRISPR-Cas9 system. Nat. Pro-toc. 8, 2281–2308. 10.1038/nprot.2013.143.

102. Goldman MJ, Craft B, Hastie M, Repečka K, McDade F, Kamath A, Banerjee A, Luo Y, Rogers D, Brooks AN, et al. (2020). Visualizing and interpreting cancer genomics data via the Xena platform. Nat. Biotechnol. 38, 675–678. 10.1038/s41587-020-0546-8. [PubMed: 32444850]

103. Campeau E, Ruhl VE, Rodier F, Smith CL, Rahmberg BL, Fuss JO, Campisi J, Yaswen P, Cooper PK, and Kaufman PD (2009). A versatile viral system for expression and depletion of proteins in mammalian cells. PLoS One 4, e6529. 10.1371/journal.pone.0006529. [PubMed: 19657394]

Highlights

- A CRISPR screen identifies FAM193A as required for the response to MDM2 inhibition
- FAM193A is necessary for p53 stabilization and downstream transcriptional responses
- FAM193A interacts with the RING domain of MDM4 and destabilizes MDM4
- FAM193A expression is associated with better prognosis in multiple cancer types

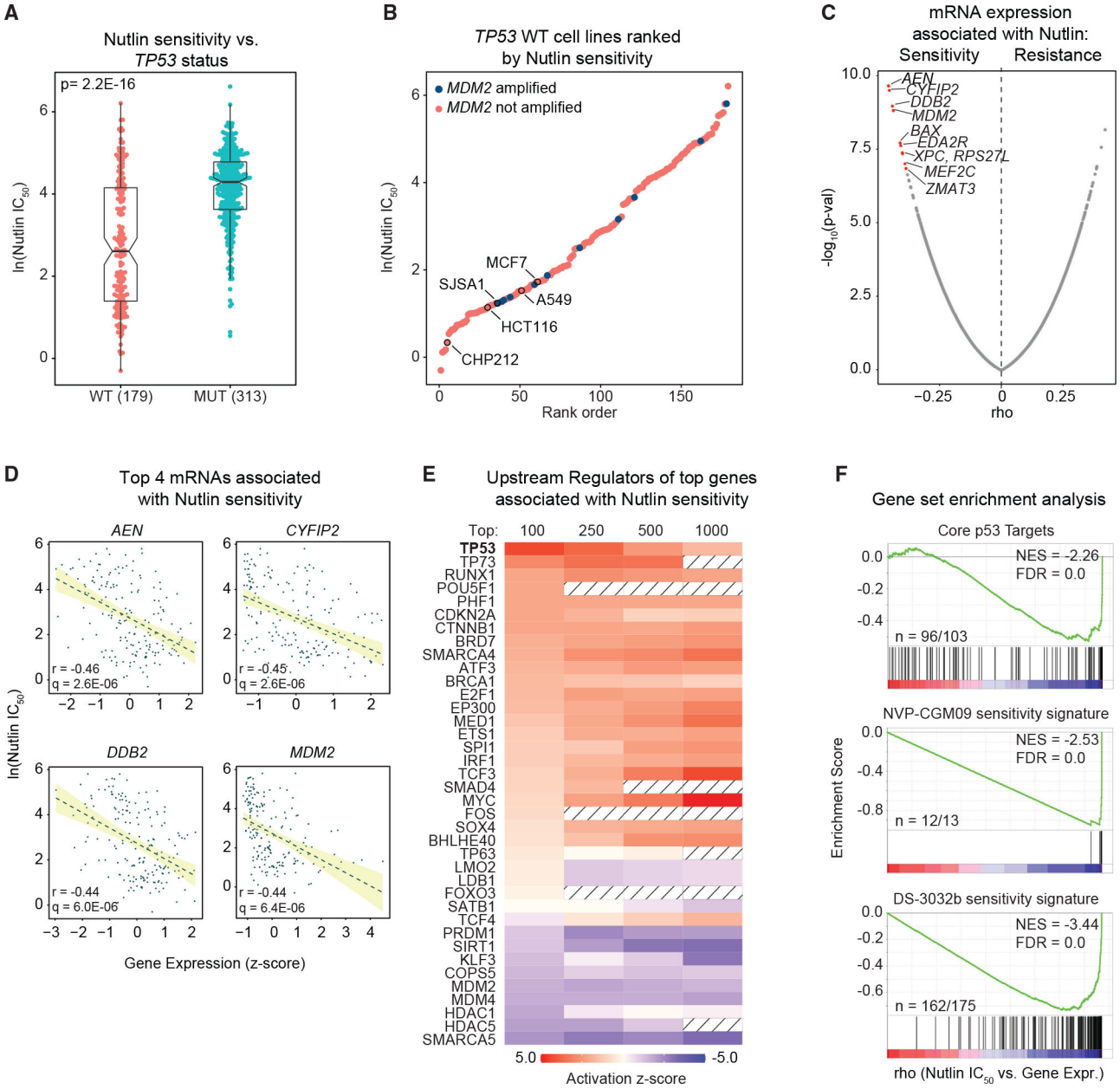

Figure 1. Sensitivity to MDM2 inhibitors is associated with high basal activity in the p53 network

(A) Distribution of Nutlin IC_{50} values (micromolar, natural logarithm) of *TP53* WT and *TP53* mutant cell lines. Drug sensitivity data were obtained from the GDSC database. The number of biological replicates for the *TP53* WT and MUT cell lines was 179 and 313, respectively; IC_{50} values were calculated based on data obtained from 2 technical replicates as described previously.[38] The notches indicate medians, and whiskers extend to the largest/smallest value but no further than the 1.5× IQR (interquartile range) from the hinge. Statistical significance was calculated with unpaired two-sample Wilcoxon test.

(B) Ranking of *TP53* WT cell lines based on their sensitivity to Nutlin, with demarcation of cells carrying *MDM2* gene amplification. Also annotated on the rank plot are cell lines used in this study. The number of biological replicates for cell lines with amplified and without

amplified *MDM2* was 11 and 168, respectively; IC_{50} values were calculated based on data obtained from 2 technical replicates as described previously.[38]

(C) Distribution of p values (negative $\log_{10}$) and Spearman correlation coefficients (rho) calculated between Nutlin IC_{50} and gene expression (basal RNA levels, obtained from the GDSC database) in *TP53* WT cell lines. Nutlin IC_{50} data were obtained based on biological and technical replicates for *TP53* WT cell lines as described in (A). Gene expression profiling was performed for each cell line in 1 replicate.[40] The top 10 genes with highest negative correlations and smallest p values are highlighted in red.

(D) Scatter plots and linear regression curves between Nutlin IC_{50} (micromolar, natural logarithm) values and RNA levels for the 4 most negatively correlated genes highlighted in (C). Statistical analysis was performed as indicated in (C), and p values were adjusted with the Benjamini-Hochberg procedure (q values). Biological and technical replicates for IC_{50} values and expression data are as described in (C).

(E) Upstream transcriptional regulators predicted by the Upstream Regulator tool of the Ingenuity Pathway Analysis (IPA) software of the top 100, 250, 500, and 1,000 genes with the highest negative correlations shown in (C).

(F) Gene set enrichment analysis (GSEA) comparison between correlations shown in (C) and (l)core genes induced by Nutlin[6] or (2) a gene signature predictive of sensitivity to the MDM2 inhibitor NVP-CGM09 or (3) a gene signature predictive of sensitivity to the MDM2 inhibitor DS-3032b.

See also Figure S1.

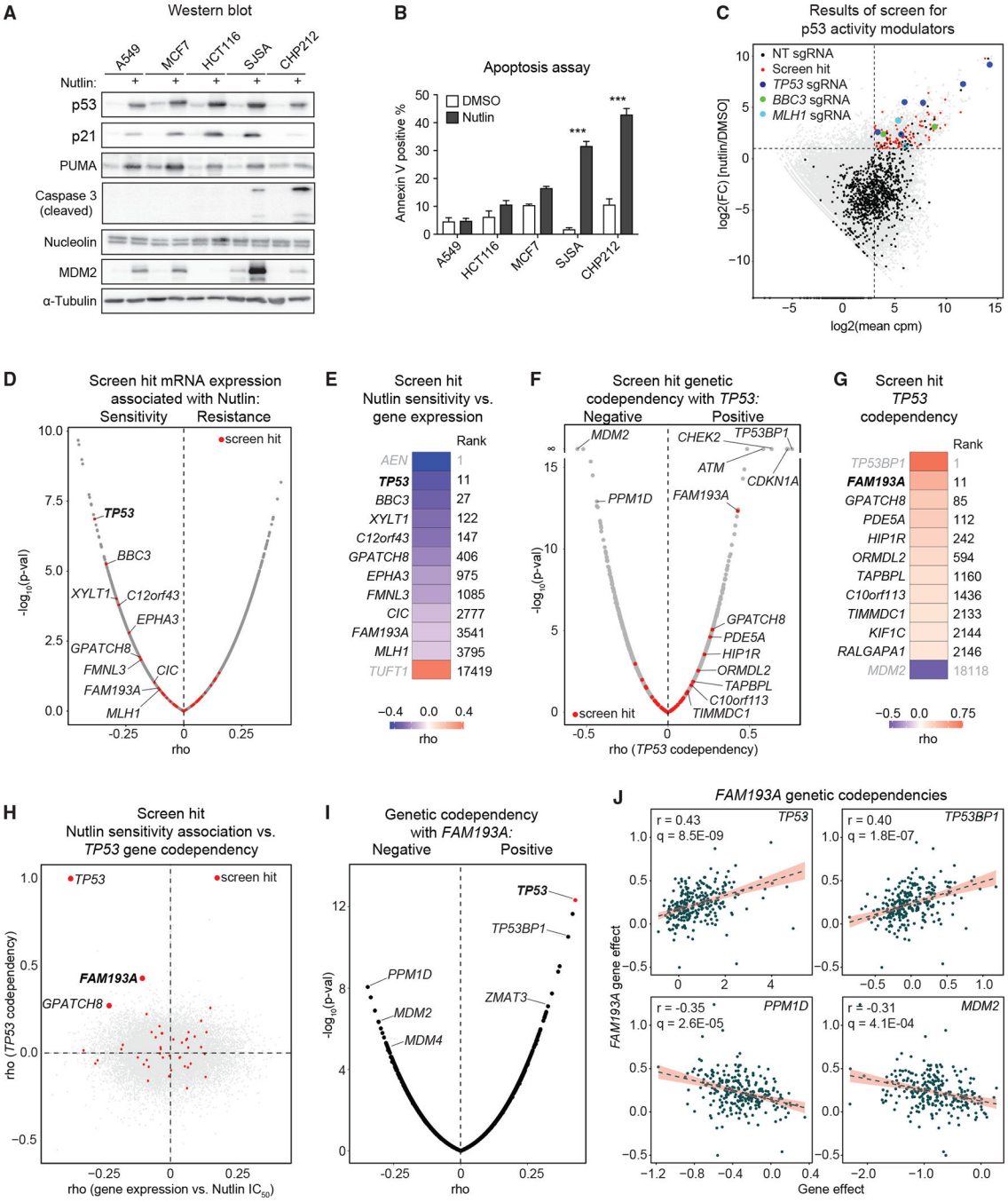

Figure 2. A genetic screen for positive regulators of p53 function

(A) Western blot analysis of components of the p53 network and apoptosis markers in A549, MCF7, HCT116, SJSA, and CHP212cellstreated for48 h with 10 μM Nutlin.

(B) Apoptosis induction measured by Annexin V binding in cells treated with Nutlin as in (A). The graph represents the average of 3 biological replicates ± SEM. Statistical analysis was performed with ANOVA with post hoc Tukey test.

(C) Scatterplot of mean counts per million (cpm) and fold changes (FCs) of sgRNAs detected by next-generation sequencing following 2 rounds of Nutlin or DMSO treatment

(2 biological replicates each). A dashed line indicates cutoff values of the screen analysis pipeline. Red, blue, green, and cyan dots indicate sgRNAs targeting genes that passed the final criterium of a minimum of 2 sgRNAs enrichment per gene.

(D) Volcano plot showing p values (log_{10}) and Spearman's correlation coefficients calculated for Nutlin IC_{50} values and gene expression levels (as presented and with statistics calculated as in Figure 1C). Genes targeted by sgRNAs enriched in the CRISPR screen are marked in red.

(E) Heatmap of correlation coefficients of the top-10 screen hits listed on the plot shown in (D).

(F) Volcano plot showing p values (log_{10}) and Spearman's correlation coefficients for *TP53* codependencies calculated with data obtained from the DepMap database (261 *TP53* WT cell lines with 4 technical replicates each were used to calculate gene effect scores[42]). Top positive and negative *TP53* codependent genes are labeled. Additionally, CRISPR screen hits are indicated in red, and the top 10 *TP53* codependent CRISPR hits are highlighted.

(G) Heatmap of *TP53* codependency rho values and gene ranks of top-10 screen hits listed on the plot shown in (F).

(H) Scatterplot for correlation coefficients of gene expression levels and Nutlin IC_{50} values (on the x axis) vs. *TP53* gene codependencies (on the y axis). CRISPR screen hit genes are highlighted in red.

(I) Volcano plot of *FAM193A* gene codependencies (rho vs. p values). *TP53* and major p53 regulators and effectors found as top positive and negative *FAM193A* codependent genes are labeled on the plot (biological and technical replicates as described in F).

(J) Scatterplots with linear regression lines of *FAM193A* gene effects plotted against *TP53, TP53BP1, PPM1D,* and *MDM2* gene effects as calculated in (I) with p values adjusted with the Benjamini-Hochberg procedure (q values, biological and technical replicates as described in F).

See also Figure S2.

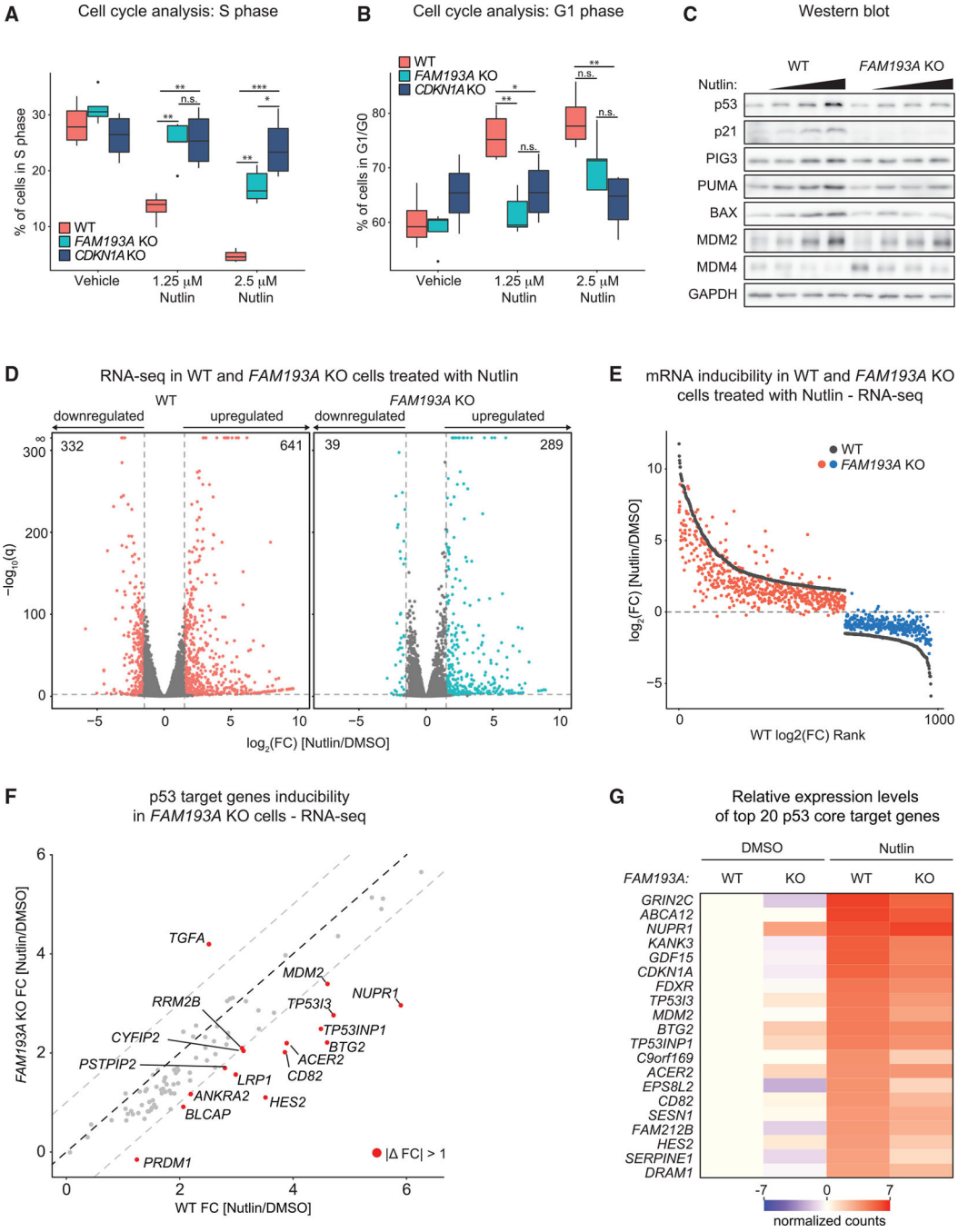

Figure 3. FAM193 is a positive regulator of p53 activity

(A) Boxplot of the percentages of cells in S phase of the cell cycle in control non-targeting (WT), *FAM193A* KO, and *CDKN1A* KO cells treated with the indicated doses of Nutlin for 24 h. The percentage of cells in S phase was measured through immunofluorescence detection of incorporated bromodeoxyuridine (BrdU). The plot represents a summary of data from independent single cell clones (biological replicates represented by individual single cell clones are 4, 5, and 4 per group for the WT, *FAM193A* KO, and *CDKN1A* KO, respectively; each sample was obtained from 2 technical replicates). The horizontal line

represents the median, and whiskers extend to the largest/smallest value but no further than the 1.5× IQR from the median. Statistical analysis was performed with ANOVA with post hoc Tukey test.

(B) Plot of the percentage of cells in G1 phase in samples as described in (A). Quantification of cells in G1 was based on detection of DNA content (stained with propidium iodide [PI]) and immunofluorescence detection of BrdU.

(A and B) *p < 0.05, **p < 0.01, ***p < 0.001.

(C) Western blot analysis of p53, p53 target genes, and MDM4 in nontargeting control (WT) and *FAM193A* KO CHP212 cells treated with vehicle or0.625,1.25, or 2.5 μM Nutlin for 24 h.

(D) Volcano plots of gene expression changes (FCs [$\log_2$FC; Nutlin/DMSO] vs. adjusted p value [q]) induced upon 12 h of 10 μM Nutlin treatment. Genes that did not pass gating for subsequent analysis (with $|\log_2 FC| < 1.5$ and/or $q > 0.05$) are marked in gray.

(E) Rank plot of mRNA FCs of DEGs in *FAM193A* WT cells (black dots). Corresponding FCs in *FAM193A* KO cells are marked in red (for upregulated genes) and blue (for downregulated genes).

(F) Scatterplot of expression FCs in WT and *FAM193A* KO cells of core p53 target genes. Regions of the plane above and below the gray dashed lines include data points with differences in FCs between WT and *FAM193A* KO that are greater than 1.

(G) Heatmap of relative expression levels of top 20 Nutlin-induced p53 core target genes.

(D–G) RNA-seq was performed on 2 biological replicates per condition.

See also Figure S3.

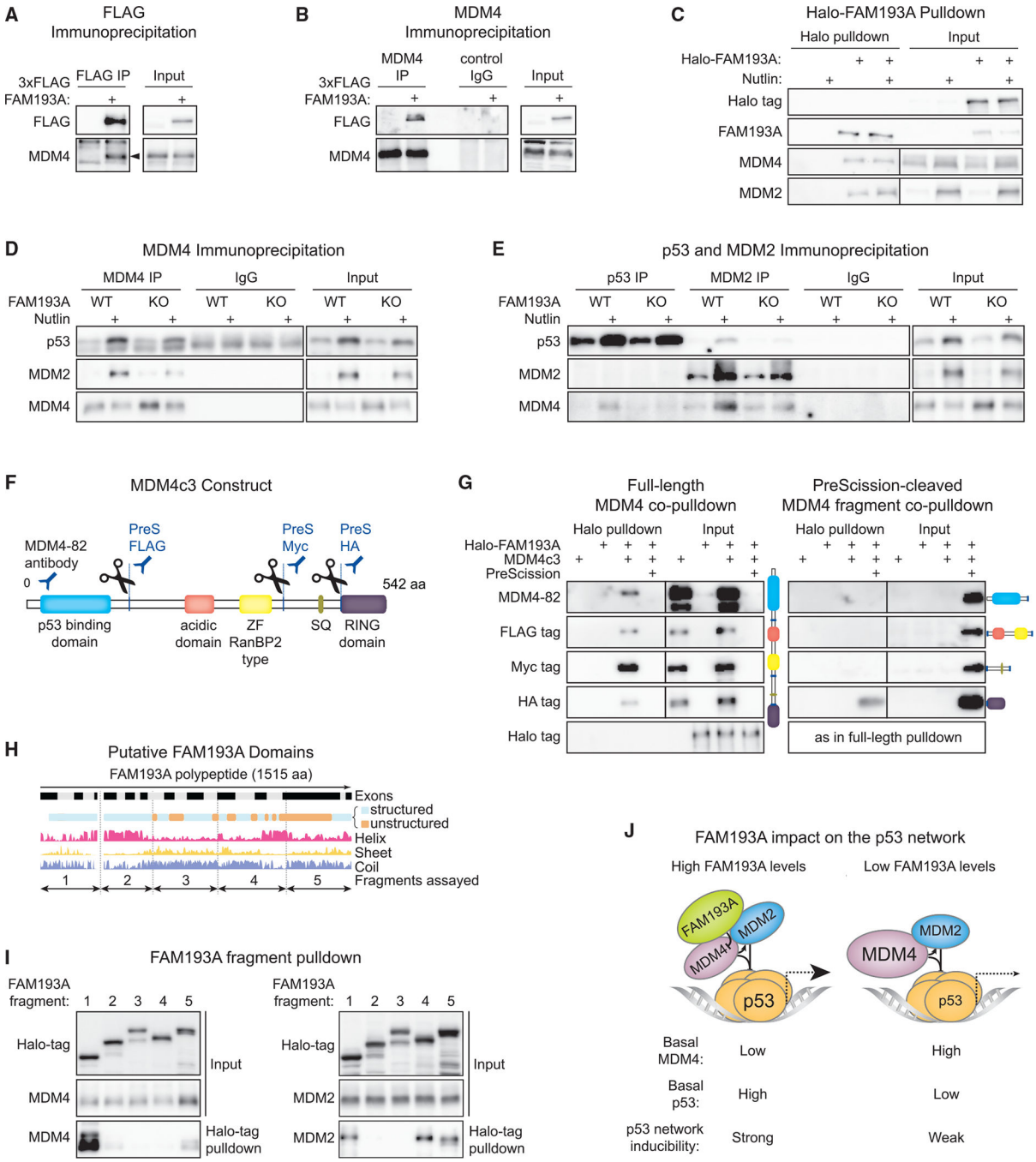

Figure 4. FAM193A interacts with the RING domain of MDM4

(A) Western blot analysis post Immunoprecipitation of 3×FLAG-FAM193A In CHP212 cells showing co-immunoprecipitation of MDM4 along with FAM193A.

(B) Western blot analysis of samples immunoprecipitated with an MDM4 antibody showing co-immunoprecipitation of 3×FLAG-FAM193A along with MDM4 in CHP212 cells.

(C) Western blot analysis of Halo-FAM193A pulldown in transfected HCT116 cells in Nutlin-treated and control cells reveals formation of a ternary complex between FAM193A, MDM4, and MDM2.

(D and E) Western blot analysis of MDM4 immunoprecipitation or (E) p53 and MDM2 immunoprecipitation in non-targeting control (WT) and *FAM193A* KO (KO) CHP212 cells treated with Nutlin.

(F) Schematics of the MDM4c3 construct. The MDM4 open reading frame was modified to include insertions of 3 PreScission (PreS) protease cleavage sites. Additionally, 3 of the4 fragments were tagged with FLAG, myc, or HA tags. Digestion of MDM4c3 with PreS leads to generation of4protein fragments containing (1)the p53-binding domain recognized bythe MDM4–82 monoclonal antibody, (2) the acidic and zinc-finger(ZF) RanBP2-type domains labeled with a FLAG tag, (3) the domain containing the SQ motif labeled with a myc tag, and (4) the RING domain labeled with an HA tag.

(G) Western blot analysis following pull-down of Halo-tagged FAM193A in transfected HEK293FT cells along with full-length MDM4c3 or with PreS-cleaved MDM4c3 fragments reveals interaction between FAM193A and the MDM4 RING domain.

(H) Secondary structures of FAM193A protein predicted by MobiDB[51] with demarcated FAM193A fragments assayed for MDM4 and MDM2 interaction.

(I) Co-pulldown of Halo-tagged FAM193A fragments (as indicated in H) with MDM4 (ectopically expressed) or MDM2 (expression induced with 10 μM Nutlin for16 h) in HCT116 cells.

(J) Proposed model of FAM193A function in supporting the p53 transcriptional program. See also Figure S4.

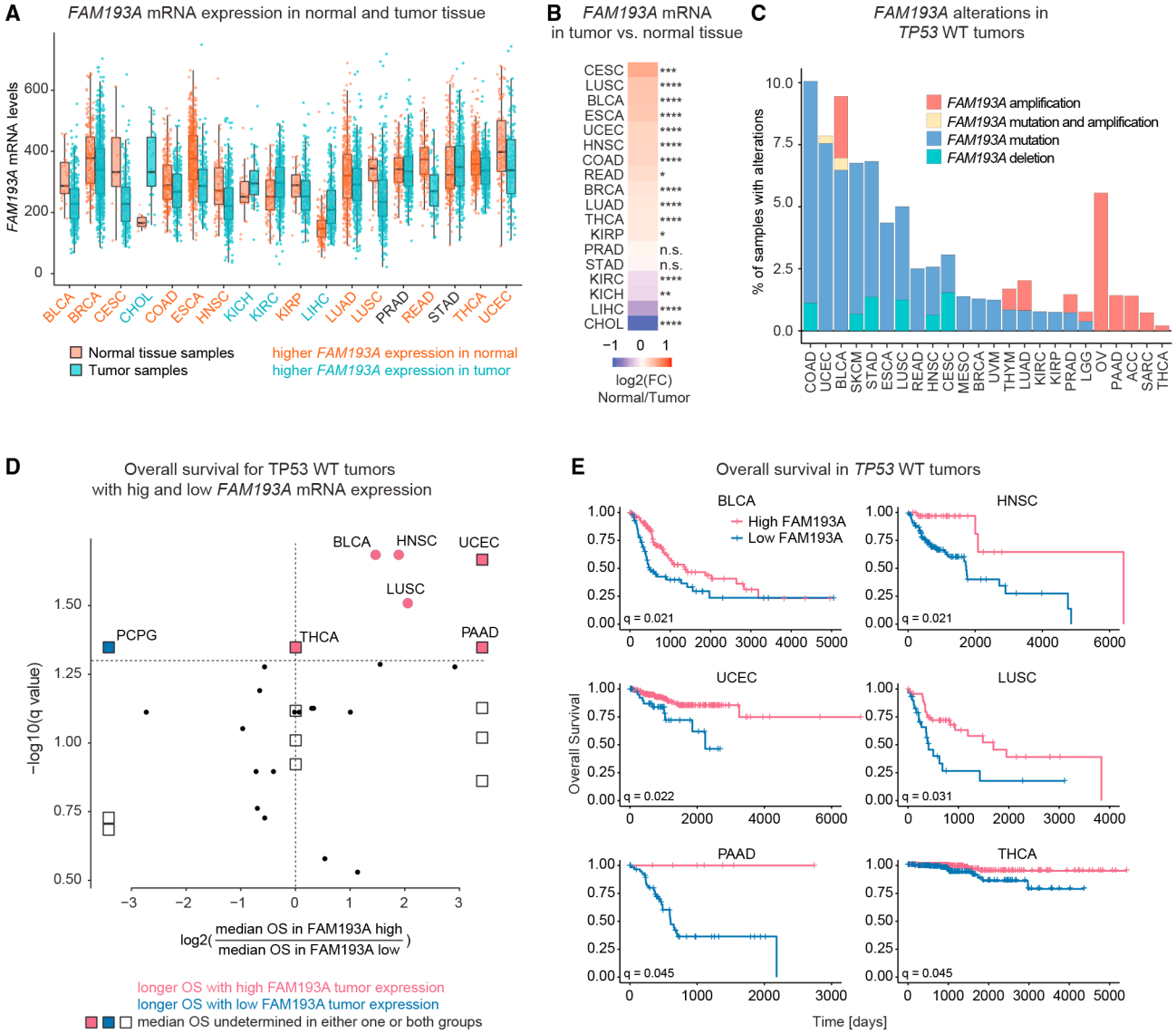

Figure 5. High FAM193A expression is associated with better prognosis in multiple cancer types

(A) *FAM193A* normalized gene expression levels(FPKM) in tumor samples and corresponding normal tissues (from the GTEx and TCGA databases). Cancer types marked in orange or teal are tumor-normal tissue pairs with significant differences in *FAM193A* expression. The horizontal lines represent the median, and whiskers extend to the largest/smallest value but no farther than the 1.5× IQR from the median. Statistical analysis was performed with Wilcoxon rank-sum test with Benjamini-Hochberg correction. The number of normal and tumor tissues profiled are as follows (cancer type: normal/tumor): BLCA: 28/362, BRCA: 199/982, CESC: 13/259, CHOL: 9/31,COAD: 235/285, ESCA: 670/183, HNSC: 97/460, KICH: 25/60, KIRC: 104/475, KIRP: 29/236, LIHC: 163/295, LUAD: 372/503, LUSC: 154/426, READ: 153/87, STAD: 225/380, THCA: 371/441, UCEC: 105/141.

(B) Heatmap of FCs of mean *FAM193A* mRNA expression between normal and cancer tissues depicted in (A). Statistical significance is denoted by asterisks (*p < 0.05, **p < 0.01, and ***p < 0.001).

(C) Distribution of *FAM193A* alterations (mutations, deletions, and/or amplifications) by cancer type in *TP53* WT tumors (data source: TCGA Pan-Cancer Atlas Studies).

(D) Plot of overall survival (OS) ratios of patients with high *FAM193A*-expressing tumors vs. low *FAM193A*-expressing tumors (all tumors are *TP53* WT) and log rank test p values adjusted with the Benjamini-Hochberg procedure (q values).

(E) Kaplan-Meier plots of OS of patients with *TP53* WT tumors with high or low expression of *FAM193A* in cancer types that surpassed the q value cutoff marked in (D). The numbers of *FAM193A* high- and low-expressing tumors are as follows(cancer type: normal/tumor): BLCA: 129/70, HNSC: 35/118, UCEC: 273/44, LUSC: 49/30, PAAD: 7/61,THCA: 306/176.

See also Figure S5.

KEY RESOURCES TABLE

REAGENT or RESOURCE	SOURCE	IDENTIFIER
Antibodies		
BAX	Cell Signaling Technology	Cat#2772; RRID:AB_10695870
BID	Cell Signaling Technology	Cat#2002; RRID:AB_10692485
BrdU	Santa Cruz Biotechnology	Cat#sc-32323; RRID:AB_626766
Cleaved Caspase-3	Cell Signaling Technology	Cat#9661; RRID:AB_2341188
Caspase-8	Cell Signaling Technology	Cat#9746; RRID:AB_2275120
GAPDH	Santa Cruz Biotechnology	Cat#sc-365062; RRID:AB_10847862
FAM193A	Abcam	Cat#ab122832; RRID:AB_11128856
FLAG tag M2	Sigma-Aldrich	Cat#F1804; RRID:AB_262044
HA-tag	Cell Signaling Technology	Cat#3724; RRID:AB_1549585
Halo-tag	Promega	Cat#G9211; RRID:AB_2688011
Histone H2B	Cell Signaling Technology	Cat#12364; RRID:AB_2714167
Lamin B1	Cell Signaling Technology	Cat#13435; RRID:AB_2737428
MDM2	Santa Cruz Biotechnology	Cat#sc-965; RRID:AB_627920
MDM4	Bethyl Laboratories Inc.	Cat#A300-287A; RRID:AB_263407
MDM4 (−82)	Sigma-Aldrich	Cat#M0445; RRID:AB_532256
myc-tag	Cell Signaling Technology	Cat#2278; RRID:AB_490778
nucleolin/C23	Santa Cruz Biotechnology	Cat#sc-8031; RRID:AB_670271
p21	Santa Cruz Biotechnology	Cat#sc-817; RRID:AB_628072
p53	Millipore Sigma	Cat#OP43; RRID:AB_10682938
PIG3	Santa Cruz Biotechnology	Cat#sc-166664; RRID:AB_2303666
PUMA	Santa Cruz Biotechnology	Cat#sc-374223; RRID:AB_10987708
PUMA	Cell Signaling Technology	Cat#12450; RRID:AB_902228
α-Tubulin	Sigma Aldrich	Cat#T9026; RRID:AB_477593
Wip1	Santa Cruz Biotechnology	Cat#sc-376257; RRID:AB_10986000
goat anti-mouse IgG, HRP linked	Biorad	Cat#1721011; RRID:AB_11125936
goat anti-rabbit IgG, HRP linked	Biorad	Cat#1706515; RRID:AB_11125142
horse anti-mouse IgG, HRP linked	Cell Signaling Technology	Cat#7076; RRID:AB_330924
goat anti-rabbit IgG, HRP linked	Cell Signaling Technology	Cat#7074; RRID:AB_2099233
Normal Rabbit IgG	Cell Signaling Technology	Cat#2729; RRID:AB_591709
Normal Mouse IgG	Santa Cruz Biotechnology	Cat#sc-2025; RRID:AB_737182
Rabbit anti-Mouse IgG (H + L) Cross-Adsorbed Secondary Antibody, Alexa Fluor 488	ThermoFisher Scientific	Cat#A-11059; RRID:AB_142495
Bacterial and virus strains		
NEB Stable Competent E. coli (High Efficiency)	New England Biolabs Inc.	Cat#C3040
Chemicals, peptides, and recombinant proteins		
Annexin V, FITC	Life Technologies	Cat#A13199
Anti-FLAG M2 Magnetic Beads	Sigma-Aldrich	Cat#M8823

REAGENT or RESOURCE	SOURCE	IDENTIFIER
Doxycycline hyclate, 98%	ThermoFisher Scientific	Cat#446060050
Dynabeads Protein G	ThermoFisher Scientific	Cat#10004D
Mouse IgG-Agarose	Sigma-Aldrich	Cat#A0919
Nutlin	Cayman Chemicals	Cat#10004372
5-Fluorouracil	Sigma Aldrich	Cat#F6627
Cycloheximide	EMD Millipore	Cat#239763
Carfilzomib (PR-171)	Selleck Chemicals	Cat#S2853
PreScission Protease	Cytiva	Cat#27-0843-01
ProTEV Plus	Promega	Cat#V6101
Thiazolyl Blue Tetrazolium Bromide	Sigma-Aldrich	Cat#M5655
cOmplete Mini	Roche	Cat#11836153001
Aprotinin	Gold Biotechnology	Cat#A-655-25
Trypsin Inhibitor	MP Biomedicals	Cat#101113
Leupeptin hemisulfate	Research Products International	Cat#L22035
Pepstatin	BioReagents	Cat#BP267125
Sodium fluoride	Mallinckrodt Chemicals	Cat#7636-04
Sodium orthovanadate	Sigma-Aldrich	Cat#S6508
DAPI	Sigma-Aldrich	Cat#D9542
Molecular Probes ProLong Gold Antifade Mountant	ThermoFisher Scientific	Cat#P36934
Lipofectamine 3000 Transfection Reagent	ThermoFisher Scientific	Cat#L3000008
Polyethylenimine Linear, MW 25000	Polysciences	Cat#23966
Alt-R S.p. Cas9 Nuclease V3	Integrated DNA Technologies Inc.	Cat#1081058
Critical commercial assays		
TRI Reagent™ Solution	Invitrogen	Cat#AM9738
DNeasy Blood and Tissue Kit	Qiagen	Cat#69506
Agilent RNA 6000 Pico Kit	Agilent Technologies, Inc.	Cat#5067-1513
Agilent High Sensitivity DNA Kit	Agilent Technologies, Inc.	Cat#5067-4626
SYBR Select Master Mix for CFX	ThermoFisher Scientific	Cat#4472954
HaloTag Mammalian Pull-Down System	Promega	Cat#G6504
TOPO™ TA Cloning™ Kit for Sequencing	Invitrogen	Cat#K457501SC
CloneJET PCR Cloning Kit	Thermo Scientific	Cat#K1231
SF Cell Line 4D-Nucleofector X Kit S	Lonza	Cat#V4XC-2032
Deposited data		
CHP212 FAM193A WT/KO RNA-seq (GSE189133)	Gene Expression Omnibus	https://www.ncbi.nlm.nih.gov/geo/query/acc.cgi?acc=GSE189133
CRISPR Screen (GSE189132)	Gene Expression Omnibus	https://www.ncbi.nlm.nih.gov/geo/query/acc.cgi?acc=GSE189132
Experimental models: Cell lines		
CHP212	ATCC	Cat#CRL-2273; RRID:CVCL_1125

REAGENT or RESOURCE	SOURCE	IDENTIFIER
A549	CU Anschutz Cell Technologies Shared Resource	Cat#CVCL_0023; RRID:CVCL_0023
HCT116	CU Anschutz Cell Technologies Shared Resource	Cat#CVCL_0291; RRID:CVCL_0291
MCF7	CU Anschutz Cell Technologies Shared Resource	Cat#CVCL_0031; RID:CVCL_0031
SJSA	CU Anschutz Cell Technologies Shared Resource	Cat#CVCL_1697; RRID:CVCL_1697
HEK293FT	ATCC	Cat#CRL-3249; RRID:CVCL_6911
H4	ATCC	Cat#HTB-148; RRID:CVCL_1239
94T778	ATCC	Cat#CRL-3044; RRID:CVCL_U613
Oligonucleotides		
For RT-qPCR primers, see Table S6.	Integrated DNA Technologies Inc.	N/A
For ChIP-qPCR primers, see Table S7.	Integrated DNA Technologies Inc.	N/A
For primers used in CRISPR screen, see Table S8.	Integrated DNA Technologies Inc.	N/A
For primers/oligonucleotides used for knockout cell line generation/genotyping, see Table S9.	Integrated DNA Technologies Inc.	N/A
For primers used for cloning and mutagenesis, see Table S10.	Integrated DNA Technologies Inc.	N/A
Recombinant DNA		
pSpCas9(BB)-2A-GFP (PX458)	Addgene (deposited by Feng Zhang)	Cat#48138; RRID:Addgene_48138
pSpCas9(BB)-2A-GFP (PX458)- HGLibA_16363 (encoding sgRNA sequence targeting *FAM193A*: TCAGAGCAACTTGCCCGCAC)	This paper	N/A
pSpCas9(BB)-2A-GFP (PX458)- HGLibA_16364 (encoding sgRNA sequence targeting *FAM193A*: TATGCAGTTCCCACGTCACT)	This paper	N/A
pSpCas9(BB)-2A-GFP (PX458)- HGLibB_16341(encoding sgRNA sequence targeting *FAM193A*: CGAGCTTGCAGATGACACAC)	This paper	N/A
pSpCas9(BB)-2A-GFP (PX458)- HGLibA_64384/ HGLibB_57029 (encoding control non-targeting sgRNA sequence: ACGGAGGCTAAGCGTCGCAA)	This paper	N/A
pENTR4-FLAG (w210-2)	Addgene (Eric Campeau, Paul Kaufman)	Cat#17423; RRID:Addgene_17423
pLenti CMV TetR Blast (716-1)	Addgene (deposited by Eric Campeau, Paul Kaufman)	Cat#17492; RRID:Addgene_17492
pLenti CMV/TO Puro DEST (670-1)	Addgene (deposited by Eric Campeau, Paul Kaufman)	Cat#17293; RRID:Addgene_17293
pDEST-CMV-polysite	Addgene (deposited by Robin Ketteler)	Cat#122843; RRID:Addgene_122843
pENTR4-HaloTag (w876-1)	Addgene	Cat#29644; RRID:Addgene_29644
psPAX2	Addgene (deposited by Didier Trono)	Cat#12260; RRID:Addgene_12260
pMD2.G	Addgene (deposited by Didier Trono)	Cat#12259; RRID:Addgene_12259
Human CRISPR Knockout Pooled Library (GeCKO v2)	Addgene (deposited by Feng Zhang)	Cat#1000000048
pLenti-CMV/TO-3xFLAG-FAM193A-Puro	This paper	N/A
pDEST-CMV-Halo-FAM193A-polysite	This paper	N/A

REAGENT or RESOURCE	SOURCE	IDENTIFIER
pDEST-CMV-Halo-FAM193A-fragment 1 (1–250)-polysite	This paper	N/A
pDEST-CMV-Halo-FAM193A-fragment 2 (251–566)-polysite	This paper	N/A
pDEST-CMV-Halo-FAM193A-fragment 3 (567–882)-polysite	This paper	N/A
pDEST-CMV-Halo-FAM193A-fragment 4 (883–1203)-polysite	This paper	N/A
pDEST-CMV-Halo-FAM193A-fragment 5 (1199–1515)-polysite	This paper	N/A
pcDNA3.1-CMV-MDM4c3	Jiandong Chen laboratory	PMID: 27114532 PMCID: PMC4868482
pcDNA3.1-CMV-MDM4c3-deltaC	This paper	N/A
pcDNA3.1-CMV-MDM4c3-C463A	This paper	N/A
pLX304-MDM4-V5	CCSB-Broad Lentiviral Expression Collection	Cat#ccsbBroad304_00993
Software and algorithms		
R Studio (v1.4.1106) with R (v4.1.0)	RStudio, PBC	N/A
FlowJo (v10.7.2)	Becton, Dickinson & Company	N/A
GSEA software (v 4.1.0)	Broad Institute	N/A
Ingenuity Pathway Analysis (v01-19-00)	Qiagen	N/A
bcl2fastq (v1.8.4)	Illumina	N/A
FASTQC (v0.11.2)	Originator: Simon Andrews of Babraham Bioinformatics	https://www.bioinformatics.babraham.ac.uk/projects/fastqc/
fastx_toolkit (v0.0.13.2)	Originator: Hannon lab	http://hannonlab.cshl.edu/fastx_toolkit/
Bowtie2 (v2.2.3)	Originator: https://doi.org/10.1038/nmeth.1923	https://bowtie-bio.sourceforge.net/bowtie2/index.shtml
SAMtools (v0.1.19)	Originator: Heng Li	http://www.htslib.org/doc/samtools.html
FastQ Screen (v0.9.1)	Originator: Steven Wingett and Simon Andrews	https://www.bioinformatics.babraham.ac.uk/projects/fastq_screen/_build/html/index.html
fastq-mcf (v1.05)	EAutils	https://expressionanalysis.github.io/ea-utils/
Picard tools (v2.9.4)	Broad Institute	https://broadinstitute.github.io/picard/
HTSeq (v0.8.0)	Originator: Givanna Putri	https://htseq.readthedocs.io/en/master/
RSeQC (v2.6.4)	Originator: SCINet project and Iowa State University	https://rseqc.sourceforge.net/
DESeq2 (v1.18.1)	Originator: Michael Love et al.	https://bioconductor.org/packages/release/bioc/html/DESeq2.html